Stony Brook University

Cloud-Resolving Modeling of Aerosol Indirect Effects in Idealized Radiative-Convective Equilibrium with Interactive and Fixed Sea Surface Temperature

A Thesis Presented

by

CHENG-EN YANG

to

The Graduate School

in Partial Fulfillment of the

Requirements

for the Degree of

Master of Science

in

Marine and Atmospheric Science

Stony Brook University

December 2011

Stony Brook University

The Graduate School

CHENG-EN YANG

We, the thesis committee for the above candidate for the

Master of Science degree, hereby recommend

acceptance of this thesis.

Marat Khairoutdinov, Associate Professor
Institute for Terrestrial and Planetary Atmospheres
School of Marine and Atmospheric Sciences
Stony Brook University

Sultan Hameed, Professor
Institute for Terrestrial and Planetary Atmospheres
School of Marine and Atmospheric Sciences
Stony Brook University

Daniel A. Knopf, Assistant Professor
Institute for Terrestrial and Planetary Atmospheres
School of Marine and Atmospheric Sciences
Stony Brook University

This thesis is accepted by the Graduate School

Lawrence Martin
Dean of the Graduate School

Abstract of the Thesis

Cloud-Resolving Modeling of Aerosol Indirect Effects in Idealized Radiative-Convective Equilibrium with Interactive and Fixed Sea Surface Temperature

by

Cheng-En Yang

Master of Science

in

Marine and Atmospheric Science

Stony Brook University

2011

This study aims to evaluate the impact of aerosol indirect effects (AIEs) on climate variations over tropical oceans through a three-dimensional cloud-resolving model, the System for Atmospheric Modeling, in idealized radiative-convective equilibrium (RCE). In RCE framework, the interactions among radiation, convection and surface fluxes are explicitly included while the effects of the large-scale circulation on convection are ignored. The AIEs on RCE are modeled by varying the number concentration of cloud condensation nuclei (CCN), served as a proxy for the aerosol amount in the environment, over a wide range starting from pristine maritime (50 cm^{-3}) to polluted (1000 cm^{-3}) conditions. Two sets of experiments are performed: (1) with an interactive sea surface temperature (SST) predicted by the simple slab ocean model and (2) with a prescribed SST fixed at 300 K. For simplicity, both experimental sets were run with constant insolation and removed diurnal cycle. In interactive SST runs, it took several hundred days until they reach a quasi-equilibrium state.

Simulation results show that the presence of CCN causes reduced longwave cloud radiative forcing (0.6-2.5 W m^{-2}) but enhanced shortwave cloud radiative forcing (0.3-1.5 W m^{-2}) in both the interactive SST (ISST) and fixed SST (FSST) experiments. In the ISST runs with the highest CCN count, AIEs mitigate most, 1.5 K, of the greenhouse warming, 2 K, as simulated by the doubling-CO_2 experiment. It is found in both ISST and FSST runs that the increase of CCN count tends to decrease the low-cloud and high-cloud covers, but increase the middle cloud cover, enhance cloud liquid water path, snow, and graupel water paths, but reduce cloud ice and rainwater paths. The qualitative differences in hydrological cycle between the ISST and FSST are also found. In ISST runs, cooler SSTs resulted from enhanced CCN counts tend to reduce precipitable water, latent heat flux and, consequently, decrease surface precipitation rate. In the FSST runs, on the other hand, the effects are opposite, that is slightly increased latent heat flux, constant PW and increased surface precipitation rate. These differences suggest that the estimates of AIEs over tropical oceans can be quite sensitive to the choice of the fixed or interactive SST framework.

Key words: aerosol indirect effect, radiative forcing, sea surface temperature, radiative-convective equilibrium, clouds

Table of Contents

List of Tables

List of Figures

List of Abbreviations

ADEs	aerosol direct effects
AIEs	aerosol indirect effects
CCN	cloud condensation nuclei
CLD	vertical profile of cloud fraction
CRMs	cloud-resolving models
CWP	cloud liquid water path
FSSTs	experiments with a fixed sea surface temperature framework
GCMs	general circulation models
GWP	graupel water path
HCLD	high-level cloud fraction
ISSTs	experiments with an interactive sea surface temperature framework
IWP	ice water path
LCLD	low-level cloud fraction
LES	large eddy simulation models
LHF	latent heat flux
LWCF	longwave cloud radiative forcing
LWNT	net longwave radiation flux at the top of the atmosphere
LWNTC	net longwave radiation flux at the top of the atmosphere at clear sky
MCLD	mid-level cloud fraction
MCUP	updraft cloud mass flux
NC	number concentration of cloud liquid water
NG	number concentration of graupel

NI	number concentration of ice
NR	number concentration of rainwater
NS	number concentration of snow
PREC	surface precipitation
PRECIP	vertical profile of precipitation flux
PW	precipitable water
QC	mixing ratio of cloud liquid water
QG	mixing ratio of graupel
QI	mixing ratio of ice
QR	mixing ratio of rainwater
QS	mixing ratio of snow
RCE	radiative-convective equilibrium
RRTM	Rapid Radiative Transfer Model
RWP	rainwater water path
SAM	System for Atmospheric Modeling
SHF	sensible heat flux
SST	sea surface temperature
SWCF	shortwave cloud radiative forcing
SWNT	net shortwave radiation flux at the top of the atmosphere
SWNTC	net shortwave radiation flux at the top of the atmosphere at clear sky
SWP	snow water path
TCLD	total cloud fraction
THF	total heat flux

TOA	top of the atmosphere

Acknowledgments

I would like to thank my advisor, Dr. Marat Khairoutdinov, for his inspiration and his great efforts to explain things clearly during this work. Throughout my study at the Stony Brook University, he provided me with valuable advice, modeling experience, and lots of good ideas. I would not have been on the right track without him. I am also grateful to Dr. Sultan Hameed and Dr. Daniel Knopf for their invaluable comments to perfect this work.

I thank Dr. Robert Pincus and Dr. Peter Blossey for the development of SAM interface to RRTM. My work is supported by Grant NA08OAR4310544 from the National Oceanic and Atmospheric Administration to Stony Brook University. This work could not have been possible without the computing resources provided by the New York Center for Computational Science, which is a joint venture of Stony Brook University and Brookhaven National Laboratory.

I am greatly indebted to my fellow colleagues, Parama Mukherjee, Minghua Zheng, Zhenhai Zhang, Wei Yuan, and Shu Meir Wang for providing a stimulating and enjoyable environment in which to learn and grow. I am especially grateful to Parama Mukherjee who helped to refine my English writing. I am also grateful to the secretaries in the School of Marine and Atmospheric Sciences for assisting me in many different ways during my study at Stony Brook University.

Lastly and most importantly, I wish to thank my beloved family, especially my parents. Without their encouragement and support I would not have completed this thesis. To them I dedicate this thesis.

CHAPTER 1 INTRODUCTION

Aerosols play an important role in climate variations by scattering and absorbing radiation and consequently altering the radiative energy budget. The aerosol effects can be classified as direct effects and indirect effects on the radiative budget at play. The aerosol direct effects (ADEs) represent the scattering and absorption of radiation by aerosols (Figure 1.1), which are responsible for changes of radiative balances in the Earth system. Compared to ADEs, the aerosol indirect effects (AIEs) can be further grouped into the first indirect effect, or Twomey effect (Twomey, 1974), and the second indirect effect, or Albrecht effect (Albrecht, 1989). Twomey effect describes that an increase in the number concentration of the cloud condensation nuclei (CCN) induces a higher cloud albedo. Albrecht effect is associated with the changes of cloud lifetime and precipitation efficiency. The more aerosols are introduced into the atmosphere, the longer cloud lifetime, more cloud liquid water content, resulting in increased cloud height (Pincus and Baker, 1994), and reduced precipitation efficiency (Albrecht, 1989).

The Fourth Assessment Report (AR4) of the Intergovernmental Panel on Climate Change (IPCC, 2007) has shown a negative feedback on radiative forcing by both ADEs and AIEs (Figure 1.1). However, the complicated interactions between aerosols and clouds cause their radiative forcing on climate to be highly uncertain. The magnitude can be as large as the net positive radiative forcing by greenhouse gases (Figure 1.2). These uncertainties originating from the subgrid-scale processes in cloud microphysics and aerosol properties make the estimation of AIEs very difficult.

One way to understand the complicated relations between aerosols, clouds and climate is through model simulations. Aerosol-cloud parameterization in general circulation models (GCMs) is the most common method to examine the impact of AIEs on climate variations

(Abdul-Razzak and Ghan, 2002; Nenes and Seinfeld, 2003; Liu and Penner, 2005; Hoose et al., 2010). For example, Rotstayn and Penner (2001) showed a magnitude of -1.32 W m^{-2} for the second indirect effect and a total indirect effect of -2.57 W m^{-2} with sea surface temperature (SST) fixed; Rotstayn and Liu (2009) found that AIEs varied from -0.38 to -0.65 W m^{-2} from GCM simulations; Lohmann and Feichter (2005) summarized that the first aerosol indirect effect induced a -0.5 to -1.9 W m^{-2} variation of radiative forcing at the top of the atmosphere (TOA) and -0.3 to -1.4 W m^{-2} for the second aerosol indirect effect; Kristjánsson (2002) found that anthropogenic aerosols caused a global-averaged indirect effect of -1.8 W m^{-2} and a 5% decrease in cloud droplet radius but a 5% increase in cloud water path; Quaas et al. (2009) found the total aerosol forcing over ocean was -1.2±0.4 W m^{-2} while AIEs were −0.7±0.4 W m^{-2}. Regardless of the wide range of AIEs, all studies consistently showed negative feedbacks on the radiative forcing by AIEs.

Nevertheless, GCM simulations are not able to resolve cloud processes explicitly, for instance the small-scale processes that comprise cloud microphysics. For those essentially, parameterizations of the subgrid-scale cloud processes are required. Hence, two-dimensional (2D) or three-dimensional (3D) large eddy simulation models (LES) and cloud-resolving models (CRMs) have been used, especially for the tropical convective cloud simulations, in order to evaluate the changes in cloud microphysics at a high-resolution spatial scale and thus the possible implications for the global climate. In this context, the CRM provide a valuable tool for understanding the climate change by resolving explicitly the interactions between tropical convection, large-scale forcing, cloud microphysics, and radiation (Tao et al., 1996, 1999).

In addition to radiative forcing, LES and CRMs have been used to explore in more detail the variations of cloud microphysics influenced by AIEs. For example, Lu and Seinfeld (2005) used

a LES to estimate AIEs over marine stratocumulus clouds through the changes of cloud optical depths. Tao et al. (2007) investigated the development of deep convective cloud systems by a 2D CRM with detailed spectral bin microphysics. Although precipitation was subdued in the beginning, they observed enhanced precipitation at a high CCN burden over the central Pacific Ocean when the model reached its equilibrium state. They concluded that evaporative cooling in the lower troposphere was the dominant factor governing the variations of precipitation. Van den Heever et al. (2011) also investigated AIEs on tropical convections using a 2D CRM with idealized conditions of radiative-convective equilibrium (RCE) fixing SST at 300 K. Morrison and Grabowski (2011) utilized a fixed-SST 2D CRM to monitor AIEs on tropical deep convections with different aerosol conditions. One of their conclusions showed that surface precipitation was insensitive to aerosols in the presence of large-scale forcing in the model.

Although simulations of 2D CRMs are similar to that of 3D CRMs (Xu et al., 2002), 3D CRMs have shown better ability in simulating 3D convective systems for convections under low wind speed conditions (Tomkins, 2000) while 2D CRMs tend to have transitions from shallow to deep convection too rapid (Grabowski et al., 2006). Tomkins and Craig (1999) examined the tropical oceanic convections by a 3D CRM with no large-scale flow under a fixed SST condition. They found that atmospheric relative humidity had insignificant variations and clouds also had small but nonlinear influences on the climate. Wang (2005) used a 3D CRM to study the impact of aerosols on precipitation in a tropical deep convection. In his simulation, the cloud droplet size decreased while the cloud droplet number concentration increased with aerosol concentration for stratiform clouds. These are just a few examples of the progress that CRM have made. Recent advances in super-computing enable time- and resource-consuming 3D CRMs to simulate even more complicated and small-scale cloud processes.

Since the tropical atmosphere is nearly in a radiative-convective equilibrium (RCE) state (Stephens et al., 1994), studies have shown that a RCE framework is able to examine the variations of radiation and hydrological cycles in the tropics (Xu and Randall, 1999; Tomkins and Craig, 1998a; Stephens et al., 2004b, 2008). In a RCE framework, heat is exchanged between the surface and the atmosphere through convective processes and large-scale forcing such as winds (Stephens et al., 2008). The atmospheric heating by convection is balanced by atmospheric radiative cooling in the RCE state. Moreover, an idealized RCE framework without large-scale forcing helps to identify the impact of aerosol effects on tropical convective systems (Tomkins and Craig, 1999) because convective clouds in this case develop only as a response to destabilization by radiation and surface fluxes over ocean. Hence, using a RCE framework in a CRM enables explicit resolution of the tropical convective processes, which are relevant to the real climate system to some extent (Stephens et al., 2008).

The purpose of this study is to evaluate the impact of AIEs on climate by varying the aerosol amount in the atmosphere over tropical oceans. Previous studies have examined the variations of tropical convections and AIEs on climate based on fixed SST (Tompkins and Craig, 1998a, 1999; Rotstayn and Penner, 2001; Rotstayn and Lohmann, 2002; Grabowski, 2006). However, fixed SST could induce imbalance of the heat budget at surface and the hydrological cycle if no large-scale forcing exists, i.e., AIEs could be either overestimated or underestimated. Therefore, this study performs a series of experiments with an interactive SST and a fixed SST in an idealized 3D CRM under RCE state to investigate the climate perturbations by AIEs.

Chapter 1 proposes the main goal of this study and briefly introduces the aerosol indirect effects as well as their impact on climate. Chapter 2 describes the CRM model used in this study as well as the experimental setups. Chapter 3 shows climate response due to AIEs. Chapter 4

discusses the aerosol effects on cloud properties. Chapter 5 summarizes the main findings of this study and gives the conclusion.

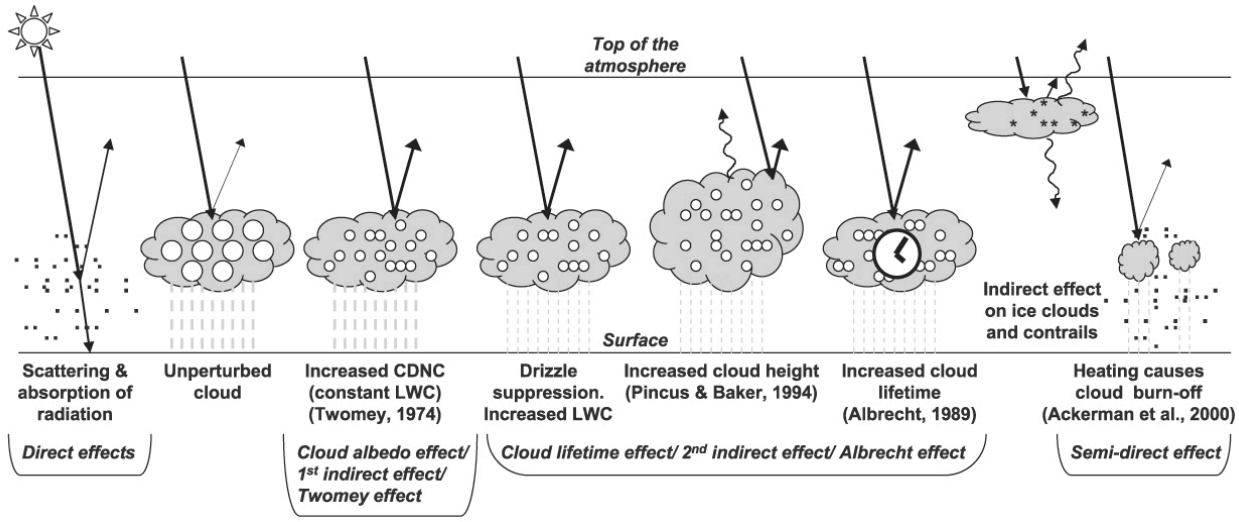

Figure 1.1. The aerosol effects on radiative mechanisms of clouds. [From the Intergovernmental Panel on Climate Change Fourth Assessment Report, 2007.]

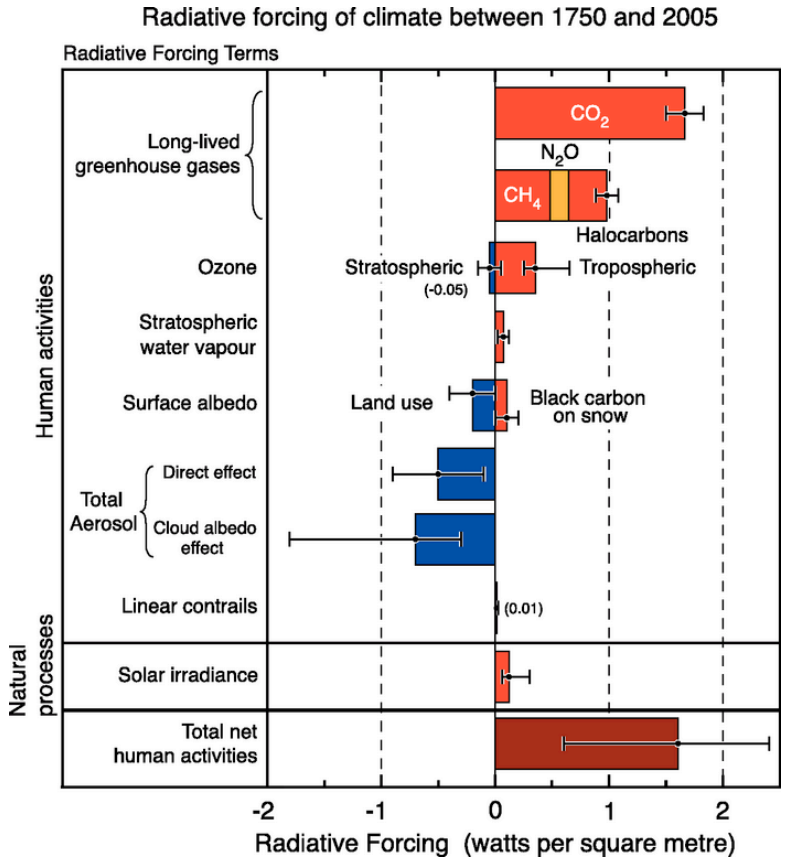

Figure 1.2. Global mean radiative forcing of climate due to various atmospheric constituents compared to pre-industrial level. [From the Intergovernmental Panel on Climate Change Fourth Assessment Report, 2007.]

CHAPTER 2 METHODOLOGY

2.1 Model Description

The System for Atmospheric Modeling (SAM) (Khairoutdinov and Randall, 2003) is a three-dimensional cloud-resolving model with an anelastic dynamical core solving nonhydrostatic dynamical equations. It has periodic lateral boundaries and a rigid lid at the top of the domain so that sinks and sources of momentum, mass, water, and energy are controlled during a simulation. The resolution of SAM can be from hundreds of meters to several kilometers, which is capable of simulating the formations of convective clouds. This study uses SAM version 6.8.3, which contains an updated radiative scheme and a coupled simple slab ocean model, to examine the climate changes with regards to the aerosol indirect effects (AIEs).

A slab ocean model enables the atmosphere and the ocean to interact thermodynamically. Latent heat and sensible heat exchange between the ocean surface and the atmosphere. The ocean is able to store heat as internal energy and redistribute this internal energy through horizontal transport. In this manner, energy is conserved during the course of a simulation within the domain. The ocean model also plays an important role in SST variation. Experiments can be performed either by prescribing SST at a fixed temperature throughout a simulation or by altering SST interactively determined by the interactions between the atmosphere and the ocean.

The radiation scheme is adapted from an improved Rapid Radiative Transfer Model (RRTM) developed by Atmospheric and Environmental Research, Inc. for both the shortwave (RRTMG-SW, version 3.8) and the longwave (RRTMG-LW, version 4.84) spectrums. RRTM computes radiation based on instantaneous temperature, vapor and cloud fields from SAM outputs. These fields are applied to the computation of radiation heating rates associated with atmospheric instability and cloud formations.

The cloud microphysics uses a two-moment bulk microphysical scheme from Morrison et al. (2005). This scheme includes kinetic equations for the mixing ratio and the number concentration of hydrometeors, which determine the conversion rates of the hydrometeors and the associated latent heat release in SAM. The number concentrations and the mixing ratios of three prognostic thermodynamic variables in SAM are the liquid- and ice-water static energy, the total non-precipitating water (cloud liquid water, cloud ice), and the total precipitating water (rainwater, snow, graupel). The Newtonian damping is applied to the upper third of the domain to reduce gravity wave reflection and suppress the boundary interactions. The mixing ratios as well as the number concentration of five hydrometeors (cloud liquid water, cloud ice, rainwater, snow, graupel) are diagnosed. The number concentration (N) of activated cloud condensation nuclei (CCN) is determined by the Twomey relation (Twomey, 1959):

$$N = CS^k ,$$

where C is the number of CCN activating at 1% supersaturation, S is the supersaturation, and k is a constant which determines the formation of droplets. A typical value of k for the equatorial maritime air masses is 0.4 (Pruppacher and Klett, 1997). This study uses different prescribed CCN number concentration as a proxy for the aerosol amount in the atmosphere.

An idealized radiative-convective equilibrium (RCE) framework is employed in SAM to simulate AIEs over tropical oceans. The main advantage of RCE is the simplicity of experimental setup wherein convection is forced by the heating differences between the atmosphere and the surface. A doubly periodic domain is usually applied to resolve the tropical convective clouds within a horizontal domain of a few hundred kilometers. Though the interactions between convection and the planetary circulation are not considered, this idealized RCE framework is still able to simulate radiation transfer, cloud microphysics, small-scale

turbulences, precipitation, and surface energy (latent heat and sensible heat) exchanges. All these processes are resolved by SAM explicitly. This study utilizes such an idealized RCE framework to investigate the aerosol indirect effects on climate.

2.2 Experimental Design

Two sets of experiments are performed to examine AIEs over tropical oceans: (1) an interactive SST predicted from the simple slab ocean model and (2) a prescribed SST fixed at 300 K. Table 2.1 shows the setup of SAM in this study. The doubly periodic domain consists of 128 × 128 grids in horizontal with 1 km resolution and 64-stretched grids in vertical with a resolution of 37.5 m near the surface to 500 m at the top (about 28 km); the slab ocean is 10 m in depth at the bottom of the domain (Figure 2.1). Time step is set to 10 seconds, which is sufficient to simulate the process of convective cloud formation in its entirety. The heating rate is updated every 45 time steps, which is equivalent to every 7.5 minutes, to determine the atmospheric instability. Results output on a daily basis. All experiments are run on New York Blue Gene supercomputer, an 18-rack IBM Blue Gene/L and 2-rack Blue Gene/P parallel supercomputer at Brookhaven National Laboratory. Each experiment uses 32 nodes (or 64 CPUs) during the course of a simulation.

In addition, an idealized RCE framework without external forcing except solar radiation is applied in this study. A constant perpetual insolation of 255 W m^{-2} without diurnal variations is imposed for all the experiments. Large-scale transports and the Coriolis force, as well as the domain mean wind, are disabled. Furthermore, the ocean body has no movement and hence horizontal transport of heat in the ocean is not considered. Only evaporation at sea surface and

precipitation from the atmosphere are allowed. Therefore, the slab ocean model interacts with the atmosphere through thermodynamic processes without any dynamical mechanism.

Vertical deep-convection and cloud formations are driven purely by radiation, surface heat and moisture fluxes. The hydrologic cycle is influenced by the evaporation at ocean surface, cloud formation, and precipitation processes in the atmosphere. Prescribed aerosol amounts in atmosphere, defined by CCN number concentration, vary from 50 to 1000 cm^{-3}, representing pristine maritime to polluted scenarios. Table 2.2 shows the CCN setups used in this study. The radiation-induced convections and cloud properties with respect to AIEs are thus examined through this idealized RCE framework.

Initial thermodynamic data is obtained from simulations performed in a RCE framework over tropical oceans by a two-dimensional SAM with coarse-resolution. The derived SST and the solar insolation are 300 K and 255 W m^{-2} at equilibrium. The carbon dioxide (CO_2) concentration is 355 ppmv, which is used as a modern CO_2 value in modeling climate changes (e.g., Govindasamy et al., 2002; Rasch et al., 2009; Kutzbach et al., 2010). All experiments run for more than 700 days as they reach or are close to quasi-equilibrium states. The outputs are smoothed by 30-day simple running mean to reduce the day-to-day perturbations. The control run for the interactive SST experiments (ISSTs) is IA100 whereas for the fixed SST experiments (FSSTs) FA100 is used.

To study AIEs on climate change, this study concerns about the differences between the control run and the other experiments by varying the CCN amount. Results are expressed in terms of departure, a value obtained by averaging the differences of the last 100-day (day 601 to day 700) outputs, i.e.,

$$Departure = \frac{\sum_{t=601}^{700} x_{2,t} - x_{1,t}}{n},$$

where $x_{1,t}$ and $x_{2,t}$ are the values of the control run and the other experimental run at time t, respectively; n is the number of days analyzed equal to 100 in this case. For a vertical profile, the departure at every level z is calculated by

$$Departure(z) = \frac{\left(\sum_{t=601}^{700} x_{2,t} - x_{1,t}\right)_z}{n}.$$

To highlight AIEs on climate changes, the departure is further converted into the fractional change, which is an averaged ratio of the departure to the value from the control run:

$$Fractional\ Change = \frac{\sum_{t=601}^{700} \frac{x_{2,t} - x_{1,t}}{x_{1,t}}}{n}.$$

With the setup described in this chapter, AIEs are thus examined by SAM. In addition, an experiment with a doubling of CO_2 scenario is performed to investigate the role AIEs play in climate changes with respect to the greenhouse warming effect.

Table 2.1. Model configurations.

Domain grids	128 x 128 x 64
Vertical height	About 28 km
Horizontal resolution	1 km
Vertical resolution	Stretching grids: 37.5 m at surface, 500 m at the top
Large-scale forcing	Radiation only; constant perpetual insolation of 255 W m^{-2}
CO_2 concentration	355 ppmv
Slab ocean depth	10 m
Time step	10 seconds
Simulation length	700 days

Table 2.2. Experimental designs. The experiment named with "I" or "F" denotes the underlying SST is interactive or fixed at 300 K. "A" represents CCN number concentration or the amount of aerosol used in an experiment. An asterisk sign denotes the control run for each experimental set. "2CO2" doubles the default CO_2 value, which is 355 ppmv, without changing any other parameters in the model.

Interactive SST experiments (ISSTs)		**Fixed SST experiments (FSSTs)**	
Case	CCN (cm^{-3})	Case	CCN (cm^{-3})
IA50	50	FA50	50
IA100*	100	FA100*	100
IA200	200	FA200	200
IA500	500	FA500	500
IA1000	1000	FA1000	1000
IA2CO2	100		

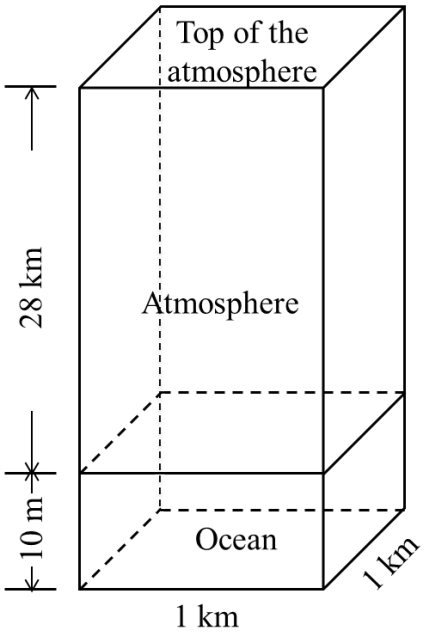

Figure 2.1. Spatial setup of a grid point used in SAM.

CHAPTER 3 AEROSOL INDIRECT EFFECTS

Every output from SAM contains more than three hundred variables and this study uses seventeen of them to examine the impact of aerosol indirect effects (AIEs) on the climate. These variables include precipitable water (PW), surface precipitation (PREC), sensible heat flux (SHF), latent heat flux (LHF), net longwave radiation flux at the top of the atmosphere (LWNT), net shortwave radiation flux at the top of the atmosphere (SWNT), net longwave radiation flux at the top of the atmosphere under clear sky (LWNTC), net shortwave radiation flux at the top of the atmosphere under clear sky (SWNTC), cloud liquid water path (CWP), ice water path (IWP), rainwater path (RWP), snow water path (SWP), graupel water path (GWP), low-level cloud fraction (LCLD), mid-level cloud fraction (MCLD), high-level cloud fraction (HCLD), and total cloud fraction (TCLD). Two additional variables, shortwave-radiative cloud forcing (SWCF, derived from SWNT and SWNTC) and longwave-radiative cloud forcing (LWCF, derived from LWNT and LWNTC), are also examined.

In this chapter, AIEs on climate changes are focus on the variations of radiation fluxes and the derived cloud radiative forcing, surface heat fluxes, and precipitation. According to the experimental setups, AIEs are evaluated based on the differences of sea surface temperature (SST) between ISSTs and FSSTs. Results are demonstrated as fractional changes of the departures from the control runs. Detailed simulation results can be found in Table A in the Appendix section**.**

3.1 Control Runs

IA100 and FA100 are the control runs in this study. Each prescribes a CCN number concentration of 100 cm^{-3} in the model run. The reason behind such a choice is not only that it represents a clean oceanic environment but also shows the minimum differences (except SWCF and HCLD) among all CCN burdens between two experimental sets (Figures 3.1, 3.2). In addition, the fractional variations, derived from the differences to the FA100 values, are less than 1% for all the variables (Figures 3.3, 3.4). Such small differences indicate that IA100 and FA100 are identical and thus all the other experiments are considered to be compared on a same basis. With this assumption, AIEs on climate changes in the other experiments of ISSTs and FSSTs are examined.

3.2 Sea Surface Temperature

SST plays an essential role in the atmospheric stability and the hydrological cycle. In the atmosphere, SST variations influence the formation of cloud droplets and thus the balance of radiation. According to the aerosol first indirect effect, increasing CCN number concentration induces more numbers but smaller sizes of cloud droplets, which in turn increases cloud albedo (Twomey, 1974). The increasing cloud albedo reflects more radiation and hence the temperature reduces. Figure 3.5 shows that SST declines significantly with respect to increasing CCN amount in ISSTs. AIEs cause a net SST cooling, ranging from 0.5 K to1.5 K, during which the CCN amount increases in value two to ten times greater than from the IA100 case in the model. Similar results are shown in previous studies using general circulation models (GCMs) or climate models. Taylor and Penner (1994) found sulfate aerosols had a cooling effect of 1.2°C over the Northern Hemisphere and 1.0°C on a global average. Mitchell and Johns (1997)

simulated a less warming effect of greenhouse gases due to the presence of sulfate aerosols in GCM simulations with variations from 0.7 K in boreal winter to 0.8 K in boreal summer.

Despite the cooling effect found in ISSTs, SST in FSSTs is forced to a fixed value at 300 K for the entire run, which causes a relatively warmer surface compared to the polluted scenarios in ISSTs as the CCN burden increases. Because all the external forcings in the model remain unchanged, it is this important constraint that causes the two experimental sets to differ significantly in their simulation results even if the CCN amount is kept the same. AIEs in each set of experiment are therefore examined and discussed in the following sections.

A doubling carbon dioxide (CO_2) experiment (IA2CO2) is also performed to examine the greenhouse warming effect with respect to the aerosol cooling effect. It is shown that the greenhouse forcing induces about 2 K increase in SST (Figure 3.6) when the model reaches quasi-equilibrium state. This value is at the lower end of global mean surface temperature predictions in IPCC AR4 for a doubling CO_2 concentration scenario (IPCC, 2007) and it is consistent with other studies (Taylor and Penner, 1994; Govindasamy et al., 2002; Rasch et al., 2009) as well. Therefore, enhancing the aerosol amount in the atmosphere can help to mitigate the greenhouse warming effect, especially at a high aerosol burden.

3.3 Radiative Fluxes

The shortwave and longwave radiation responses to AIEs in two experimental sets are quite similar in the case of shortwave radiation but not so for longwave radiation (Figure 3.7). The reasons behind similar fractional changes of departures in shortwave radiation are the imposed constant perpetual insolation and the CCN amount. The former induces almost a

constant value of SWNTC while the latter accounts for the decreasing trend in SWNT due to the first aerosol indirect effect discussed in Section 3.2.

Compared to the shortwave radiation, the longwave radiation shows completely different trends for the two sets of experiments. SST and the cloud amount play a major role in these differences. In ISSTs, LWNT and LWNTC tend to decrease with increasing CCN amount since more shortwave radiation is reflected by higher cloud albedo. SST is thus lower due to less energy reaching the ocean surface. In FSSTs, however, TCLD dominates the variation of longwave radiation since SST is fixed. The restriction of SST variation leads to negligible variations in LWNTC without clouds. When considering the presence of clouds, LWNT demonstrates a noticeable counter trend between the two sets. The controlling factor is TCLD that decreases with respect to the CCN amount (Figure 4.2). Because clouds trap longwave radiation well, more longwave radiation is able to reach the top of the atmosphere (TOA) when TCLD becomes smaller. Therefore, TCLD is responsible for the increasing trend of LWNT in FSSTs while declined SST affects the decreasing trend of LWNT in ISSTs.

3.4 Cloud Radiative Forcing

The cloud radiative forcing is another important parameter that can be employed to examine AIEs on global radiation balance. The longwave cloud radiative forcing (LWCF) and the shortwave cloud radiative forcing (SWCF) are determined by outgoing longwave radiation and incoming shortwave radiation at TOA (Charlock and Ramanathan, 1985). If F represents the longwave radiation and F_{clear} denotes the longwave radiation under a clear-sky condition while Q is the shortwave radiation and Q_{clear} denotes the shortwave radiation under a clear-sky condition, then the cloud radiative forcing can be expressed as

$$LWCF = F_{clear} - F,$$

$$SWCF = Q - Q_{clear}.$$

In this study, F and F_{clear} are represented by LWNT and LWNTC while Q and Q_{clear} are denoted by SWNT and SWNTC.

The SWCF, which is usually negative, describes the ability of clouds to scatter back shortwave radiation. Figure 3.7 shows an increasing trend of SWCF with CCN in both experimental sets. The enhancement of SWCF is more pronounced in ISSTs than FSSTs when more CCN exist in the model. AIEs enhance SWCF by 0.3-1.5 W m^{-2} in ISSTs and 0.3-1.0 W m^{-2} in FSSTs.

In contrast to SWCF, LWCF is usually positive which represents the ability of clouds to trap the longwave radiation in the atmosphere. A larger magnitude of decline in LWCF with increasing CCN amount is found in FSSTs (Figure 3.7). AIEs weaken LWCF by 0.8-2.5 W m^{-2} in FSSTs and 0.6-1.1 W m^{-2} in ISSTs. Although both sets show a decreasing trend, AIEs influence LWCF through different mechanisms. Because LWCF is controlled by LWNTC and LWNT, from Figure 3.7 there are two ways to cause the weakening of LWCF in this study: (1) LWNT increases as LWNTC is nearly constant and (2) LWNTC decreases more rapidly than LWNT does. Each way reduces the differences between LWNTC and LWNT.

From Table A in the Appendix section, it is easy to find that decreasing LWCF in FSSTs with increasing CCN is caused by increased LWNT by a magnitude of 0.5-2.8 W m^{-2}. The reason for the increased LWNT is primarily due to the reduced cloud fractions discussed in Section 3.3. In ISSTs, the rapid decline in LWNTC than LWNT is responsible for the weakened LWCF. Cooler SST with respect to the CCN amount discussed in Section 3.3 is the major cause. The magnitude of LWNTC decline in ISSTs is 0.7-2.2 W m^{-2} while that for LWNT is 0.1-1.1 W

m^{-2}. According to Section 3.3, the longwave radiation in the two sets is affected either by SST or the cloud amount. Therefore, the cloud amount should be responsible for the decreasing LWCF in FSSTs whereas SST plays the major role in LWCF decline in ISSTs.

The combination of SWCF and LWCF shows a net reduction by 0.8-2.6 W m^{-2} in ISSTs and 1.0-3.5 W m^{-2} reduction in FSSTs at TOA. The ISSTs result compares well with the simulation results from Menon et al. (2002), which concluded that AIE led to a 1.22-2.99 W m^{-2} reduction in radiation over ocean. The FSSTs result is close to Ghan et al. (2001), which simulated a negative radiative forcing of about 1.5-3.0 W m^{-2} by aerosol indirect effects. Because of this reduction in radiation at TOA, less energy reaches the surface and thus the hydrology, discussed in Section 3.6 and Chapter 4, is greatly influenced by AIEs.

3.5 Surface Fluxes

The surface heat fluxes are closely related to the variations of radiative fluxes. Although AIEs can bring about changes of the order of a few watts per meter square in the radiative fluxes, Figure 3.8 shows that the impact on SHF is small (<0.3 W m^{-2}) due to the constant perpetual insolation in the model setup. The increasing trend of the fractional changes of departures in SHF is brought about by SST and the clouds. Because SST decreases with CCN number concentration in ISSTs, a larger temperature gradient between the atmosphere and the ocean results in greater SHF. In FSSTs, the cloud amount dominates the changes of SHF since SST is fixed. The increasing trend of MCLD (Figure 4.2) is suggested to be responsible for the increasing trend of SHF through greenhouse effect despite the decreasing TCLD. Hence, the atmosphere is heated by the greenhouse effect and the temperature gradient becomes larger as more CCN implemented in the model.

The variation of LHF is dependent on the evaporation of water from the ocean. Due to the cooling effect by AIEs in ISSTs, the ocean evaporates less water into the atmosphere, which explains the decreasing trend of LHF in ISSTs (Figure 3.8). The fractional changes of departures can be up to 12.6% in the most polluted scenario (CCN=1000 cm^{-3}).

The response of LHF to AIEs in FSSTs is different from that in ISSTs. LHF increases monotonically with CCN due to the fixed SST. The water evaporates from ocean to the atmosphere at a constant rate as SST is fixed. When more CCN exist in the atmosphere, a higher number of those is able to collect water vapor and get activated as cloud droplets. The cloud droplets eventually grow up large enough to form raindrops and precipitate out. Because the precipitation process is associated with energy release, LHF increases with CCN while SST remains unchanged.

The surface total heat flux (THF), which is the combination of LHF and SHF, declines from 101.2 W m^{-2} to 96.4 W m^{-2} in ISSTs and increases from 100.7 W m^{-2} to 102.7 W m^{-2} in FSSTs. The sensitivities of THF to AIEs are higher in ISSTs than in FSSTs. The maximum fractional changes of departures for THF in ISSTs and FSSTs are -4.68% and 1.95%, respectively. This result implies that AIEs produce a net energy loss from the surface to the atmosphere in ISSTs but lead to a net gain of energy at the surface in FSSTs.

3.6 Precipitation

The difference in THF between the two sets implies the different variations in the hydrological cycle, for example precipitation. Section 3.5 has shown that LHF decreases monotonically with CCN in ISSTs. This implies less available water vapor for cloud droplets or even raindrop formation, which influences the trends of PW and PREC in ISSTs. As SST cools

with the CCN amount, both PW and PREC decrease with less water vapor in the atmosphere (Figure 3.8). Previous studies using GCMs with an interactive SST to evaluate AIEs showed a 2% reduction in global mean surface precipitation (Mitchell and Johns, 1997) and a 0.3 kg m^{-2} change in PW by averaging the results of the last 30 days (Grabowski, 2006). This study shows a similar result with an amplitude of 1.7-4.9 mm (or 4.3-12.6%) for PW perturbations and 0.17-0.51 mm day^{-1} (or 1.5-5.3%) for PREC perturbations.

On the contrary, AIEs have insignificantly impact on PW while PREC increases monotonically (Figure 3.8). The reason is that FSSTs force SST to remain at 300 K. Because the CCN amount is the only varying factor, water from the ocean evaporates into the atmosphere at a constant rate due to fixed SST. This leads to the total water vapor amount and thus PW in the atmosphere to be almost the constant in FSSTs regardless of the CCN amount.

The unchanged SST also provides sufficient water vapor for CCN to collect. The competition between CCN to gather water vapor no longer constraints the formation of cloud droplets and raindrops. The simulated PREC is of the order of 3 mm day^{-1} (Appendix, Table A), which is close to values from other studies (Kiehl and Trenberth, 1997; Rotstayn and Penner, 2001; van den Heever et al., 2011). Compared to the decreasing trend of PREC in ISSTs, AIEs cause a monotonically increasing trend with CCN about 0.02-0.06 mm day^{-1} (or 0.6-2.0%) in FSSTs. This increasing trend is also found in van den Heever et al. (2011) in which the aerosol burden was low or only computed by averaging the grid points that had precipitation.

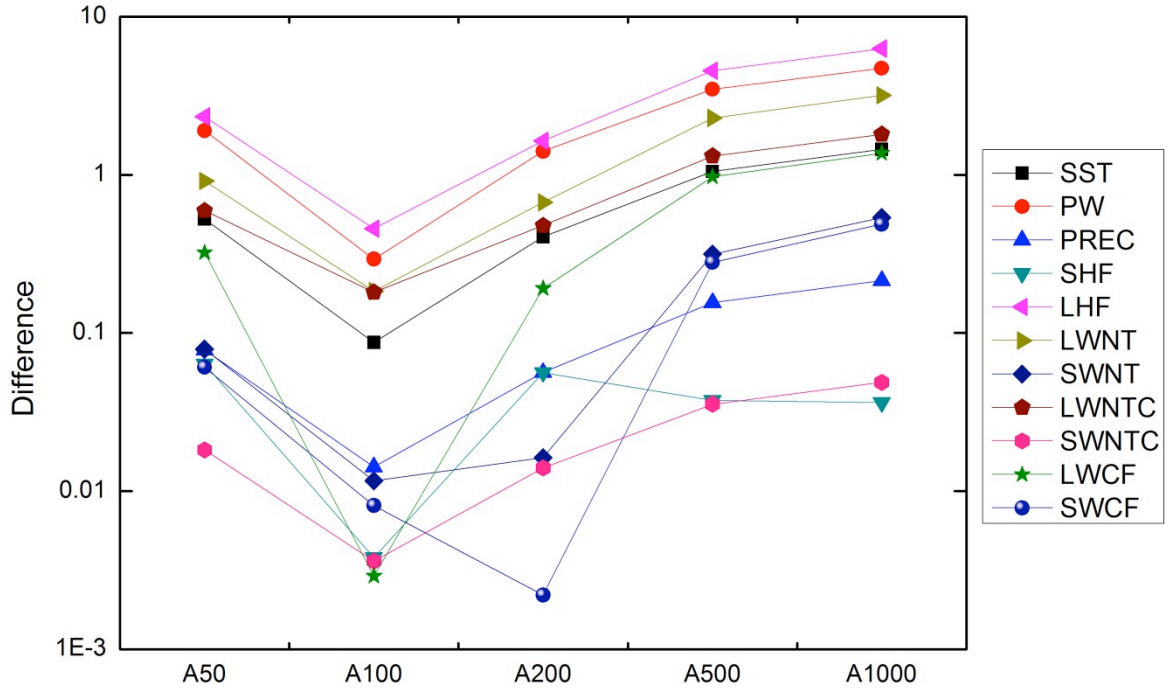

Figure 3.1. Differences of responses to aerosol indirect effects between two sets of experiments. Values are calculated by (ISST-FSST) in absolute values. The abscissa shows the scenarios of different CCN burdens.

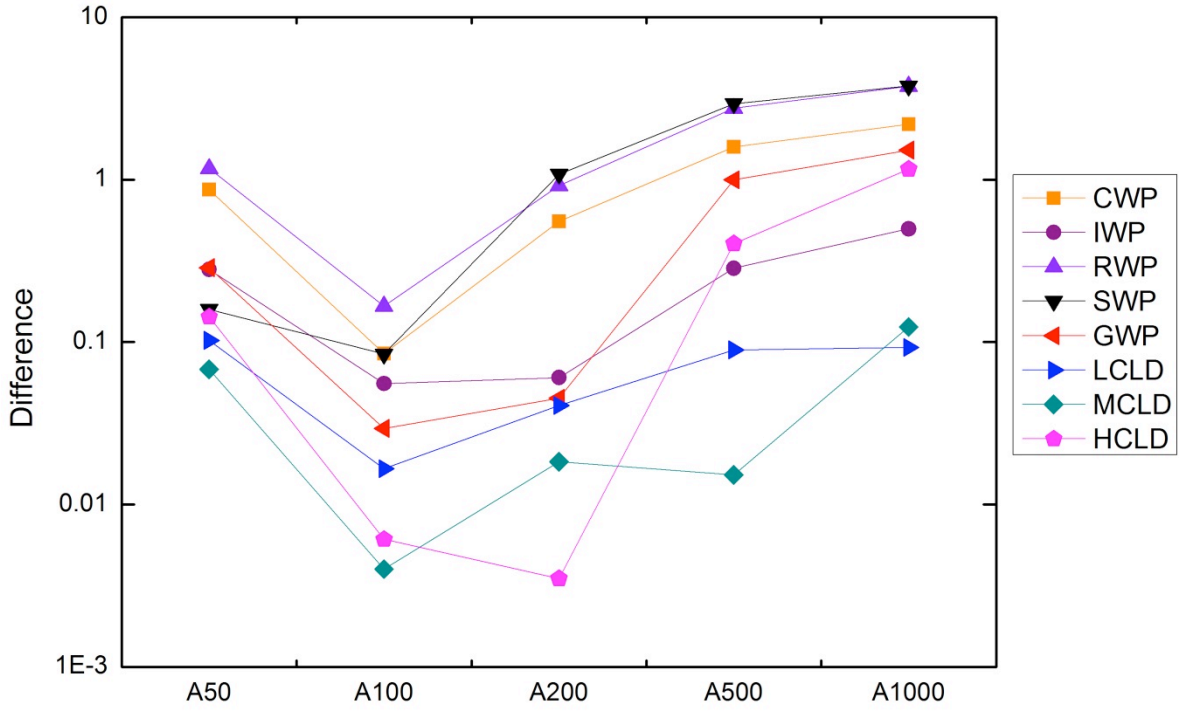

Figure 3.2. Same as Figure 3.1 except for cloud properties.

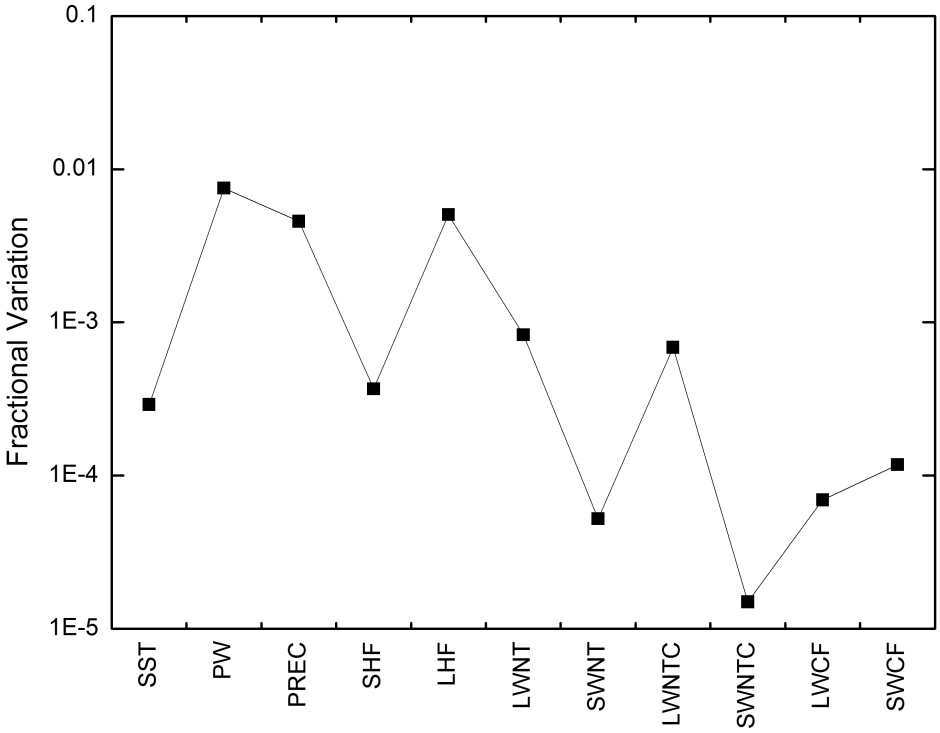

Figure 3.3. Fractional variations of the control runs. Values are calculated by (IA100-FA100) in absolute values to that of FA100. The abscissa shows different parameters.

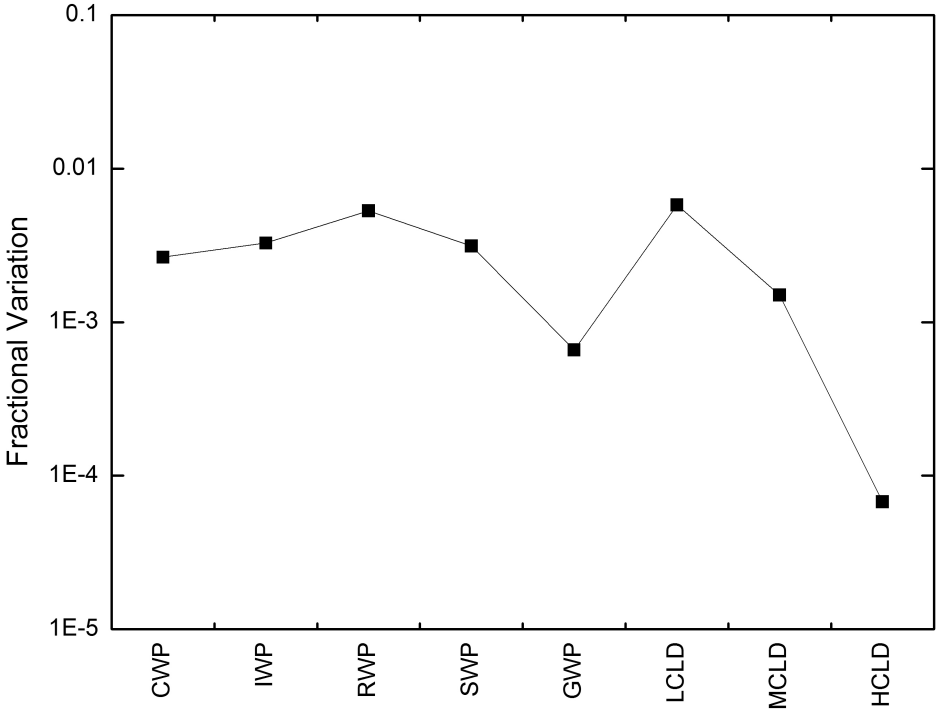

Figure 3.4. Same as Figure 3.3 except for cloud properties.

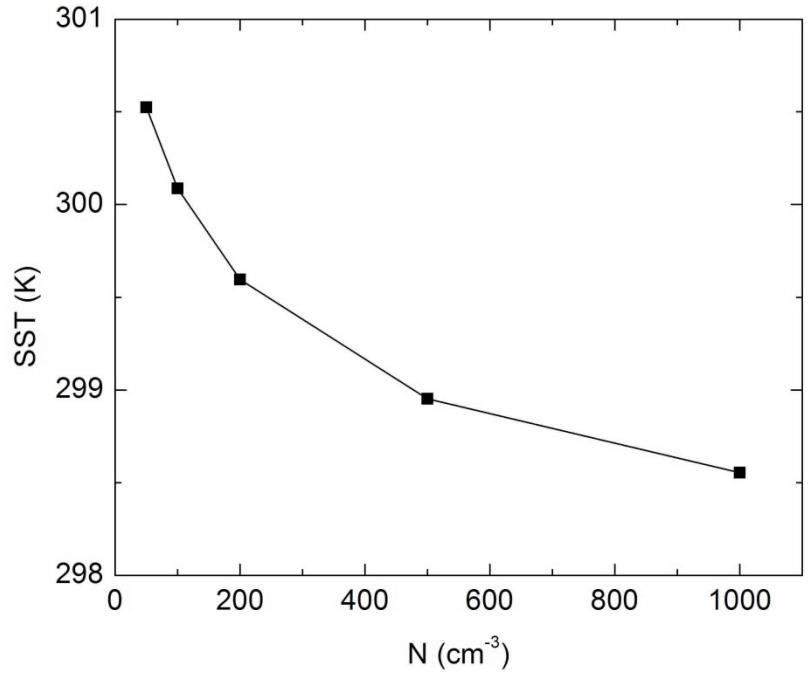

Figure 3.5. SST variations with respect to the CCN amount in ISSTs. The abscissa is the CCN number concentration. Values are calculated from the last 100-day average with 30-day running mean smoothing.

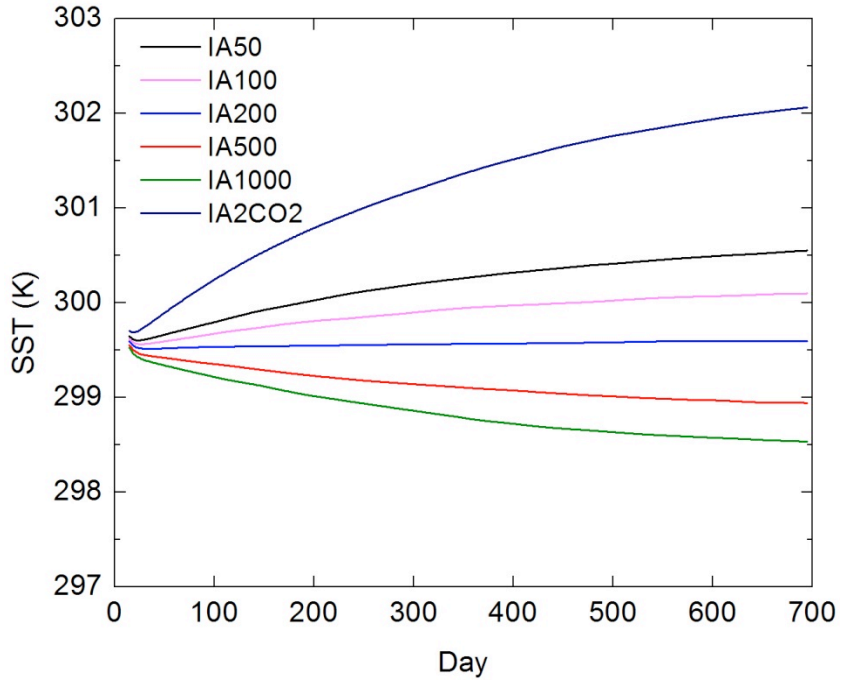

Figure 3.6. Time series of SST variations in ISSTs.

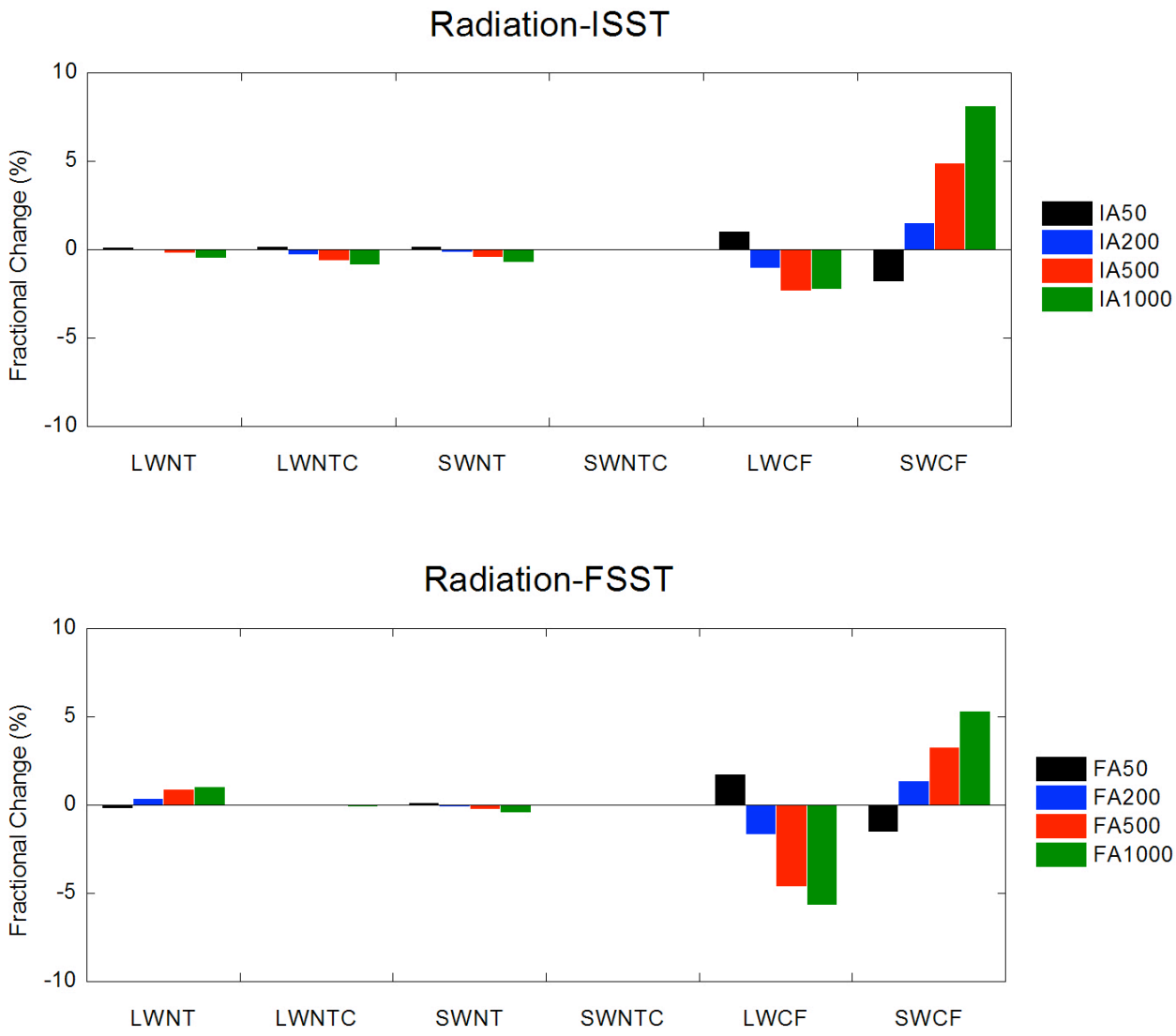

Figure 3.7. Fractional changes of departures (%) of radiation fluxes and cloud radiative forcing. LWNT: net longwave radiation at TOA; LWNTC: net longwave radiation at TOA under clear sky; SWNT: net shortwave radiation at TOA; SWNTC: net shortwave radiation at TOA under clear sky; LWCF: longwave cloud radiative forcing; SWCF: shortwave cloud radiative forcing. Upper panel: departures of ISSTs from IA100; lower panel: departures of FSSTs from FA100.

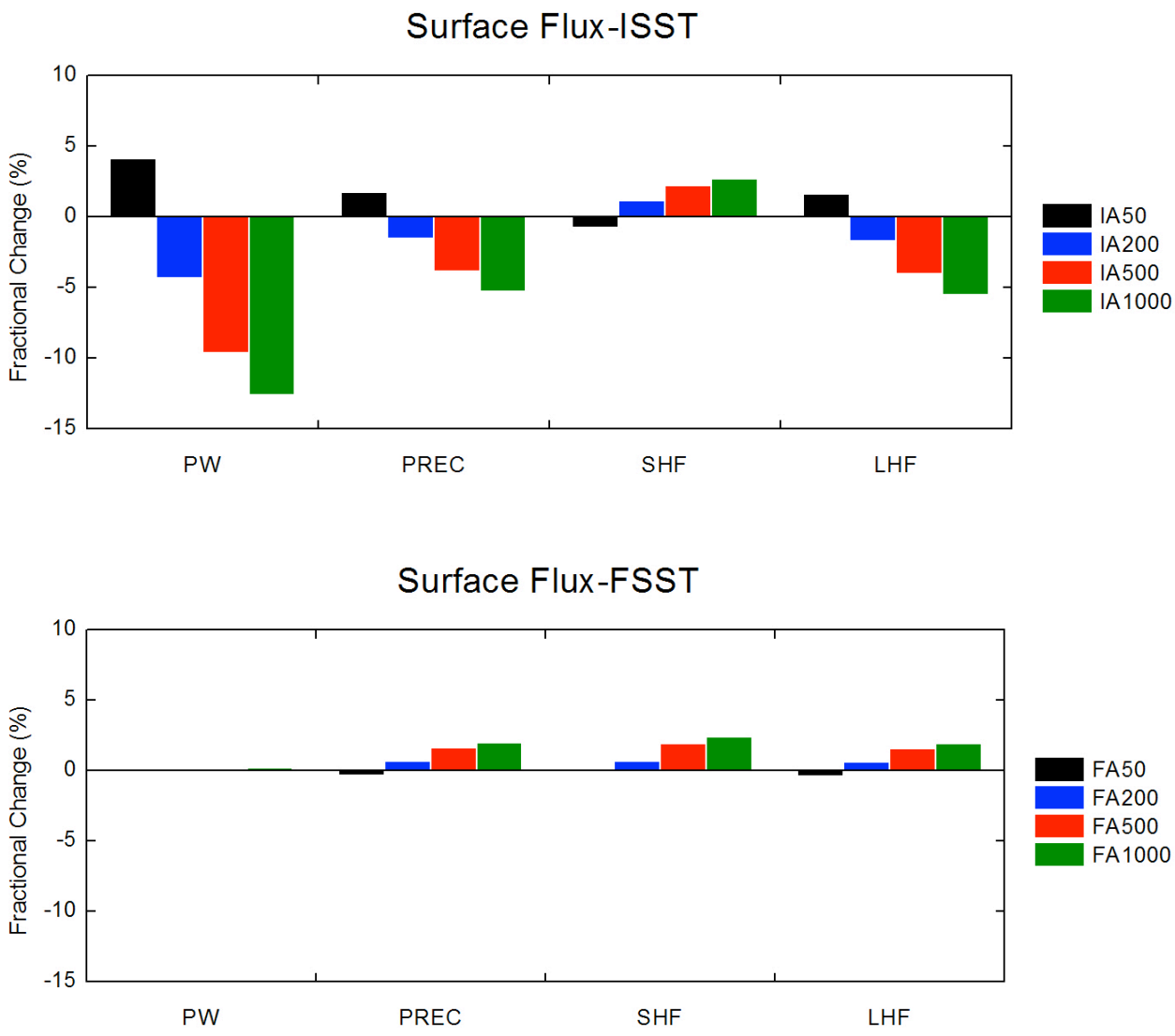

Figure 3.8. Fractional changes of departures (%) of surface fluxes. PW: precipitable water; PREC: surface precipitation; SHF: sensible heat flux; LHF: latent heat flux. Upper panel: departures of ISSTs from IA100; lower panel: departures of FSSTs from FA100.

CHAPTER 4 AEROSOL EFFECTS ON CLOUDS

In Chapter 3, it has been shown rather great differences between ISSTs and FSSTs in radiative forcing, heat fluxes, and precipitation due to aerosol indirect effects. All these variations contribute to the modifications of the hydrological cycle and consequently cloud behavior and hydrometeors. These changes in return produce a feedback on the variations of SST, radiative forcing, heat fluxes, and surface precipitation. Therefore, it is also important to examine AIEs on the properties of hydrometeors and clouds in ISSTs and FSSTs. In this chapter, the main focus is on the cloud fractions at different levels, cloud water paths, and the profiles of number concentration and mixing ratio of hydrometeors as well as the relative humidity.

4.1 Cloud Fractions

Clouds have a huge impact on climate by reflecting shortwave radiation and absorbing longwave radiation. The changes in cloud fractions contribute to the climate variations by means of altering cloud thickness and the phases of water in clouds. During daytime, a high thin cloud has low albedo, so shortwave radiation penetrates it and warms the Earth's surface; on the other hand, a thick cumulus cloud can cool the surface by absorbing most of the incoming shortwave radiation. In addition, water in different phases also influences cloud albedo and thus the variations in SST. For example, ice has smaller reflectivity than snow (Ahrens, 1998). Because cloud ice is mostly found in clouds at a higher level compared to snow, the increase of high-level cloud fraction can help warm the surface; on the other hand, the buildup of lower level clouds composed of rainwater, graupel, and snow results in a cooler SST since most of the shortwave radiation energy is absorbed, scatted, and reflected.

According to the Twomey effect (Twomey, 1974) and the Albrecht effect (Albrecht, 1989), aerosols have significant impacts on the cloud albedo and the cloud lifetime. Hence, it is necessary to investigate how cloud fractions at different heights vary with aerosols in the model. The time- and domain-averaged cloud fractions are determined by the cloud simulator from the International Satellite Cloud Climatology Project, which categorizes clouds into three vertical levels in terms of the pressure at the top of the clouds (Rossow and Schiffer, 1999). Figure 4.1 shows the high-, mid-, and low-level clouds separated by the pressure levels at 440 hPa and 680 hPa, which correspond to about 3.2 km and 6.8 km (Table 4.1) in altitude in the model.

Simulation results demonstrate that about 56% of the domain is covered by clouds and about 90% of them comes from the contribution of high-level clouds (Table A in the Appendix section) in both sets. The high-level cloud fraction (HCLD) decreases for low CCN amount and increases for high CCN episodes with a minimum value (56.3%) occurring at IA500 in ISSTs. Unlike ISSTs, HCLD in FSSTs has the maximum value in the control run, FA100, and decreases when either the CCN amount is reduced or increased. However, the changes in HCLD are different between two sets, while the low-level cloud fraction (LCLD) decreases monotonically, the mid-level cloud fraction (MCLD) increases gradually with the CCN amount in both sets.

The total cloud fraction (TCLD), which is the combination of LCLD, MCLD, and HCLD, varies similarly with CCN in both sets with a minimum value occurring at the CCN amount equal to 500 cm^{-3}. From Figure 4.2 and Table A in the Appendix section, TCLD in ISSTs is clearly affected by the trend of HCLD whereas in FSSTs it is more of a combined result of changes in all the three-levels of cloud fractions.

Although the variations of cloud fractions are different in both sets, the fractional changes of departures are small (< 5%) in HCLD and TCLD (Figure 4.2) but relatively large in MCLD (up

to 17.9%). Therefore, AIEs have small impact on the total amount of clouds in the model but they clearly affect lower level cloud formations, especially the mid-level clouds. An implication is the disparate hydrometeor properties between ISSTs and FSSTs as discussed in the next sections in this chapter. To quantify the magnitude of AIEs impact on cloud fractions at each level, the following method (van den Heever et al., 2011) is applied:

$$AIEs(CLD)\ (\%) = [1-(CLD_{min}/CLD_{max})] \times 100,$$

where CLD_{min} and CLD_{max} are the minimum and maximum values of the cloud fraction at one level in an experimental set, respectively. Generally, AIEs tend to increase MCLD but decrease LCLD, HCLD, and TCLD. For ISSTs, the magnitude of AIEs on LCLD, MCLD, HCLD, and TCLD is 10.1%, 16.9%, 2.4%, and 2.2%, respectively; for FSSTs, the magnitude is 3.8%, 15.7%, 3.1%, and 2.4%. This result once again suggests that AIEs on cloud fractions have small impact in this study, especially under the fixed SST framework.

4.2 Cloud Water Path

Column-integrated water path represents the abundance of hydrometeors in the atmosphere. Within a cloud, the cloud water path is the integral of the cloud water content in the cloud layer. This physical quantity is crucial to climate variations through its role in changing the cloud albedo, the cloud emissivity, and the cloud optical depth. For instance, the reduction of cloud liquid water path (CWP) in low-level clouds in summertime causes thinning of clouds, which induces a negative cloud optical feedback on climate (Del Genio and Wolf, 2000). In addition, the averaged ice water path (IWP) in the Tropics is found to decrease due to smaller convective mass flux under the global warming scenario, which is opposite to the increase of upper cloud

cover (Satoh et al., 2011). Therefore, the variations of cloud water paths affect the climate and vice versa.

The fact that AIEs have an impact on climate variations described in Chapter 3 and Section 4.1 demonstrates AIEs also have the potential to disturb cloud water paths and in turn the climate. Hence, this study examines AIEs on cloud water paths in perspective of CWP, IWP, rainwater path (RWP), snow water path (SWP), and graupel water path (GWP).

Simulation results show that the responses of cloud water paths to AIEs are divided into two groups (Figure 4.3): on one hand, increasing trends for CWP, SWP, and GWP and on the other hand, decreasing trends for IWP and RWP. Both groups display a monotonic trend with respect to the CCN amount in each experimental set. The opposite trends for the two groups suggest a reduction of clouds at higher and lower levels but an expansion of mid-level clouds in the model, which agrees well with the variations of cloud fractions discussed in Section 4.1. Moreover, the increasing trend of CWP in both sets implies the increase of cloud liquid water content in the model, which can be explained by the aerosol second indirect effect, i.e., increasing aerosols in the atmosphere results in higher liquid water content.

In terms of the magnitude of fractional changes, the ISSTs set shows that CWP and IWP depart little from IA100 (<10%) than that in the case of RWP, SWP, and GWP. Among all hydrometeors, SWP has the most prominent increase up to 46.1% (or 12.2 g m^{-2}) at the CCN amount equal to 1000 cm^{-3} in which RWP decreases the most about 24.3% (or 7.6 g m^{-2}). The finding that RWP and PREC (Figure 3.6) decrease with CCN clearly matches the expectations, i.e., drizzle suppression due to AIEs (Albrecht, 1989).

The fractional changes of departures of hydrometers in FSSTs have similar trends as those in ISSTs (Figure 4.3). The amplitude of the departures is enhanced with CCN for all

hydrometeors and among them RWP (negative) and SWP (positive) still have the largest fractional changes of departures. However, the magnitude of departures is relatively less for RWP and SWP but slightly increasing amplitude in CWP, IWP, and GWP in FSSTs than ISSTs. This result implies less reduction of LCLD and less increase of MCLD in FSSTs than in ISSTs. Greater reduction of IWP also supports the relatively smaller values of HCLD in FSSTs than in ISSTs.

4.3 Vertical Distributions of Cloud Properties in ISSTs

Cloud water at higher level tends to form clod cloud water (cloud ice, snow, graupel) at lower level, warm cloud water mainly exists as cloud liquid water and rainwater with relatively small amount of snow and graupel. Results in Section 4.1 have shown that AIEs cause little impact on HCLD and TCLD but relatively large impact on MCLD and LCLD, especially in ISSTs. AIEs on the variations of cloud water paths in Section 4.2 have also displayed significant decrease in IWP and RWP but increase in CWP, SWP, and GWP. However, water paths characterize AIEs in a column-integrated view that only provides information about the transformations between different water phases in the model. To better understand how hydrometeors are perturbed by the presence of CCN in the model, it is essential to examine the variations of hydrometeors at different level as well as the other cloud properties.

The departures of the mixing ratio for the hydrometeors are shown in Figures 4.4 and 4.5. At low level (below 3.2 km), cloud liquid water (QC) and rainwater (QR) decrease with increasing CCN number concentration while graupel (QG) increases and cloud ice (QI) and snow (QS) remain unchanged in both sets. Combining with the number concentration of the hydrometeors, the model simulates a scenario where rainwater reduces significantly and more

numbers but smaller sized cloud liquid water is implied in ISSTs (Figures 4.6, 4.7). Consequently, the precipitation flux (PRECIP) at low level shows a decreasing trend with increasing CCN number concentration (Figure 4.8), which is similar to previous studies (Albrecht, 1989; Lohmann and Feichter, 2005).

AIEs at middle level (3.2-6.8 km) induce a noticeable difference of the mixing ratio of hydrometeors to those at low level – only QR reduces significantly while all the other four mixing ratio fluxes of hydrometeors increase. From the updraft cloud mass flux (MCUP), representing the strength of convection in the model, shown in Figure 4.8, it is suggested that AIEs lead to stronger MCUP decreasing with height as SST cools by increasing CCN. Cloud water from the bottom of this layer is lifted up to a colder environment to form graupel, ice, and snow. In addition, stronger MCUP means a stronger updraft in which larger size of cloud water is able to suspend in the middle layer. Hence, PRECIP in this layer, mainly contributed by snow and graupel, is found to increase with the CCN amount (Figure 4.8).

At high level (above 6.8 km), there is no rainwater because of low temperature. Most cloud water exists in the forms of cloud liquid water, cloud ice, snow, and graupel. Compared to the low- and mid-level, cloud ice in the high-level plays an important role in cloud properties at this layer. Within this level, AIEs on QI show a positive effect below the cloud anvil but a negative effect at near or above the cloud anvil (Figure 4.5). One possible cause for the increasing QI is the weaker MCUP at higher layer (Figure 4.8) that cloud ice falls down to the lower layer. This weaker MCUP is also responsible for the negative response of QS and QG to AIEs at high level (Figure 4.5). As a result, AIEs on the variation of PRECIP at the high level is essentially a net negative feedback (Figure 4.8).

Considering the cloud fraction discussed in Section 4.1, HCLD is considerably influenced by the cold cloud water (cloud ice, snow, graupel), i.e., a net decreasing trend with increasing CCN at high level is expected. The relative humidity profile (RH) also provides the evidence for the reduction in LCLD and HCLD but enhanced MCLD. Because increased AIEs cool the SST and reduce MCUP, less surface water from ocean is evaporated, which results in a smaller RH. The higher RH at middle level is due to the cloud water at lower level brought up by stronger MCUP. The decline of RH at high level is affected by the decreasing cloud water and weakened MCUP. The smaller amount of cloud water leads to less water vapor and hence a reduced RH. The negative departure of MCUP also contributes to decrease of RH at high level since less cloud water is brought into this level. However, the amount of cloud water becomes smaller with height and a small perturbation in cloud water can result in a dramatic departure of RH. Therefore, the confidence level of the RH disturbance decreases with height, especially near and above the cloud anvil.

4.4 Vertical Distributions of Cloud Properties in FSSTs

AIEs on the variations of mixing ratio in FSSTs are overall smaller than those in ISSTs. It is shown that a similar QR pattern, a decreasing trend of QR with respect to the CCN number concentration, to that in ISSTs is found (Figure 4.4). All the other hydrometeors have smaller mixing ratio responses to AIEs in FSSTs than those in ISSTs (Figures 4.4, 4.5). A very small positive departure of QR at surface is simulated, which contributes to the small increasing trend in surface precipitation (Figure 3.8). In addition, the negative departures of QC, QS and QG at high level in ISSTs vanish or become positive in FSSTs. Therefore, PRECIP is slightly positive at both low and high level. Furthermore, QI in FSSTs is mainly decreased with CCN, which is

different from the increase of QI below the cloud anvil in ISSTs. It is suggested that the different MCUP patterns between ISSTs and FSSTs at high level causes the differences in QI profiles between the two sets.

In perspective of the number concentration, the departures of cloud liquid water (NC) and rainwater (NR) are almost equal to those in ISSTs (Figure 4.6). However, the patterns of the number concentration are really different for cloud ice (NI) and snow (NS). AIEs even affect a totally opposite departure of NI in FSSTs and in ISSTs. It is suggested that stronger MCUP in ISSTs than in FSSTs, especially at high CCN burden, results in this difference. Similar to ISSTs, changes of size distribution of cloud liquid water at low level and snow and graupel at high level are found. Moreover, the decrease of cold cloud water (cloud ice, snow, graupel) at higher level (around 9 km) is mainly due to the dynamic effect as shown in Section 4.3. Weaker MCUP at this level cannot provide sufficient buoyancy for large-size hydrometeors suspending in the atmosphere (Figure 4.8).

The variation of PRECIP is all positive from the surface to the cloud top (Figure 4.8). A weaker MCUP results in a reduction of PRECIP at the lower levels .The reduced PRECIP, still positive in its value, is in turn responsible for a dryer boundary layer (Figure 4.8). At higher level, the reduced PRECIP is associated with the decline in MCUP.

AIEs on RH variations in the FSSTs set are generally in consistent with those in the ISSTs at low and middle levels. Moreover, the perturbations of RH varying between positive and negative alternately with height at high level are small compared to ISSTs. This again provides that the sensitivity of climate variations in FSSTs to AIEs is smaller compared to that in ISSTs. The larger positive departures near the cloud top are not reliable due to very small amount of water vapor in this layer.

Table 4.1. The 64 levels of pressure and the corresponding height in the model.

Pressure (hPa)	Height (m)	Pressure (hPa)	Height (m)	Pressure (hPa)	Height (m)	Pressure (hPa)	Height (m)
995.7	37.5	583.4	4459	184.2	12459	46.2	20459
987.2	112.5	547.2	4959	169.4	12959	42.4	20959
978.0	194.0	512.9	5459	155.6	13459	38.9	21459
967.5	288.1	480.3	5959	142.7	13959	35.7	21959
95.6	395.4	449.4	6459	130.9	14459	32.8	22459
941.9	520.1	420.0	6959	120.1	14959	30.1	22959
925.9	557.5	392.2	7459	110.2	15459	27.7	23459
907.1	843.8	365.9	7959	101.0	15959	25.5	23959
884.1	1062	340.9	8459	92.6	16459	23.4	24459
856.4	1332	317.2	8959	84.9	16959	21.5	24959
823.1	1665	294.8	9459	77.8	17459	19.8	25459
785.5	2055	273.7	9959	71.3	17959	18.2	25959
745.0	2493	253.6	10459	65.4	18459	16.8	26459
703.1	2966	234.7	10959	59.9	18959	15.5	26959
661.5	3459	216.9	11459	54.9	19459	14.3	27459
621.4	3959	200.1	11959	50.4	19959	13.2	27959

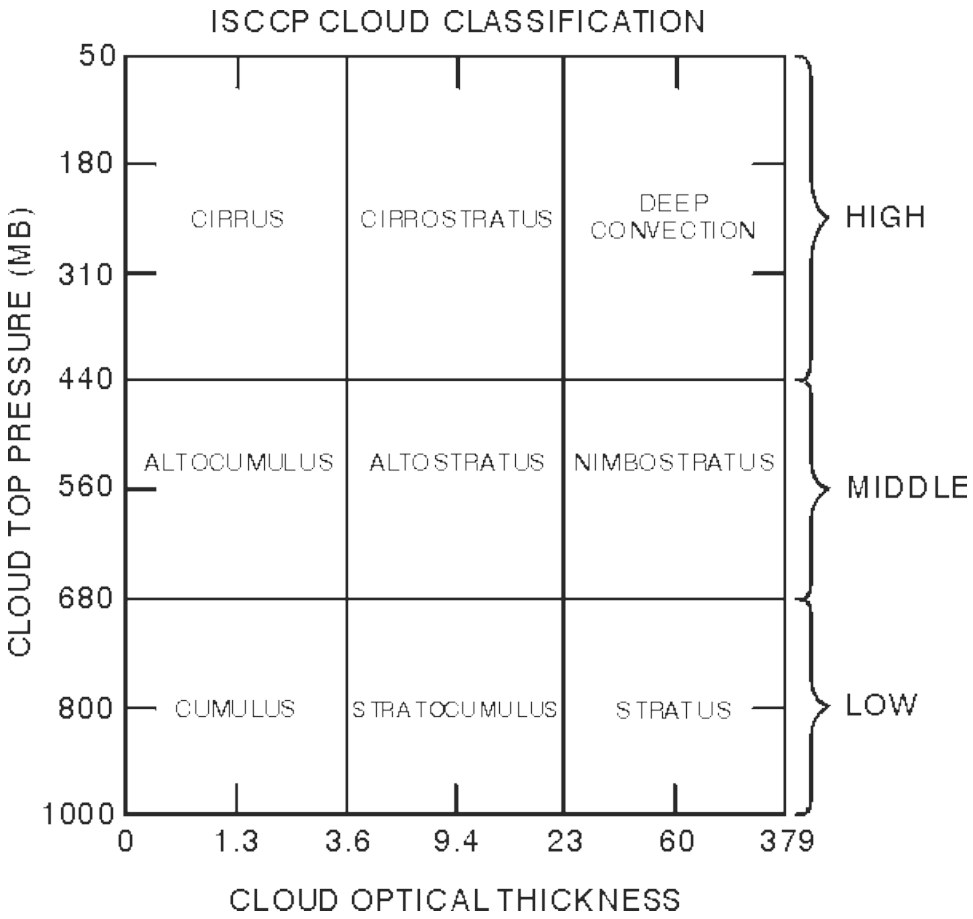

Figure 4.1. ISCCP cloud types classification. [From Rossow, W.B. and R.A. Schiffer, 1999.]

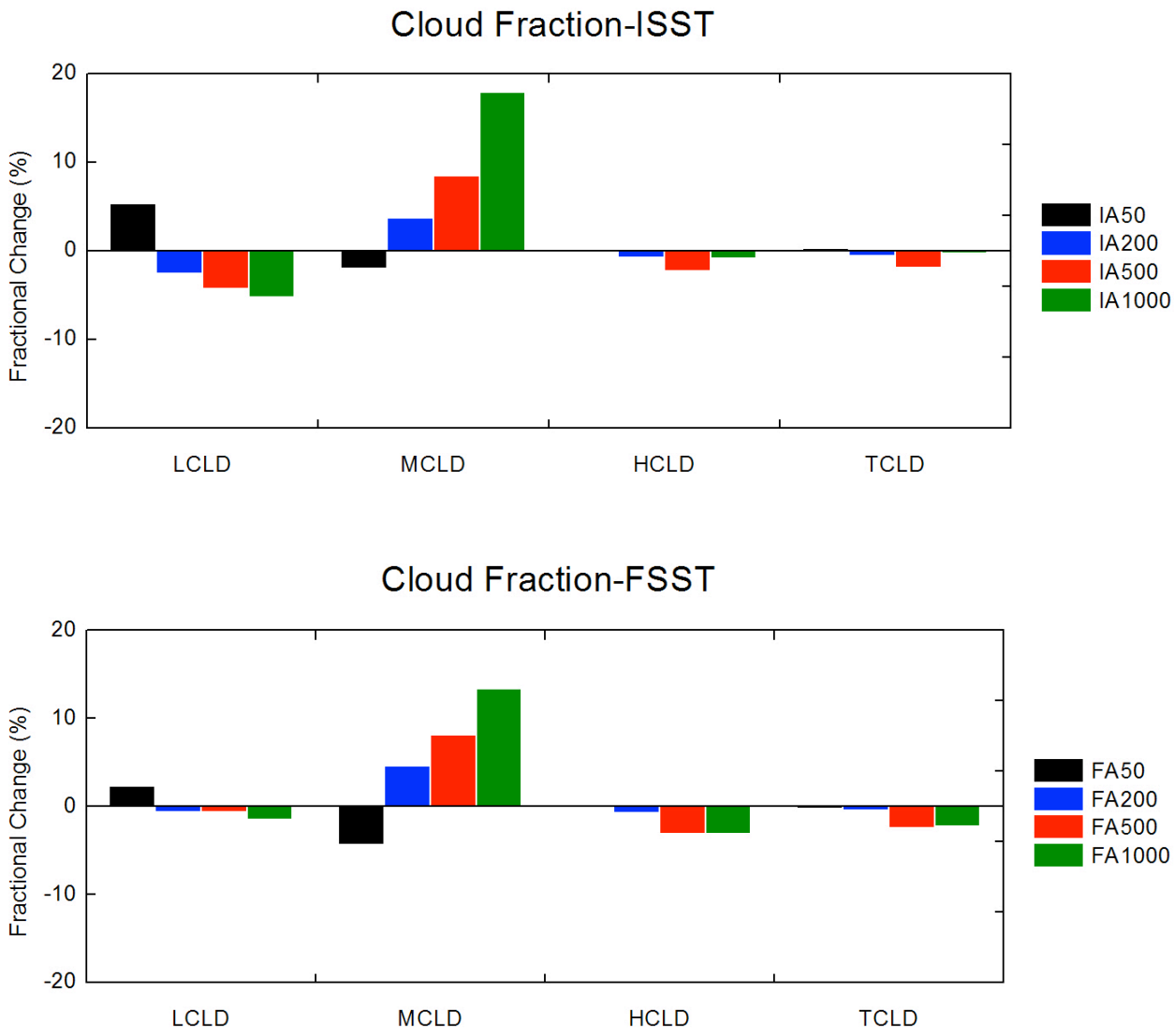

Figure 4.2. Fractional changes of departures (%) of cloud fractions. Upper panel: departures of ISSTs from IA100; lower panel: departures of FSSTs from FA100.

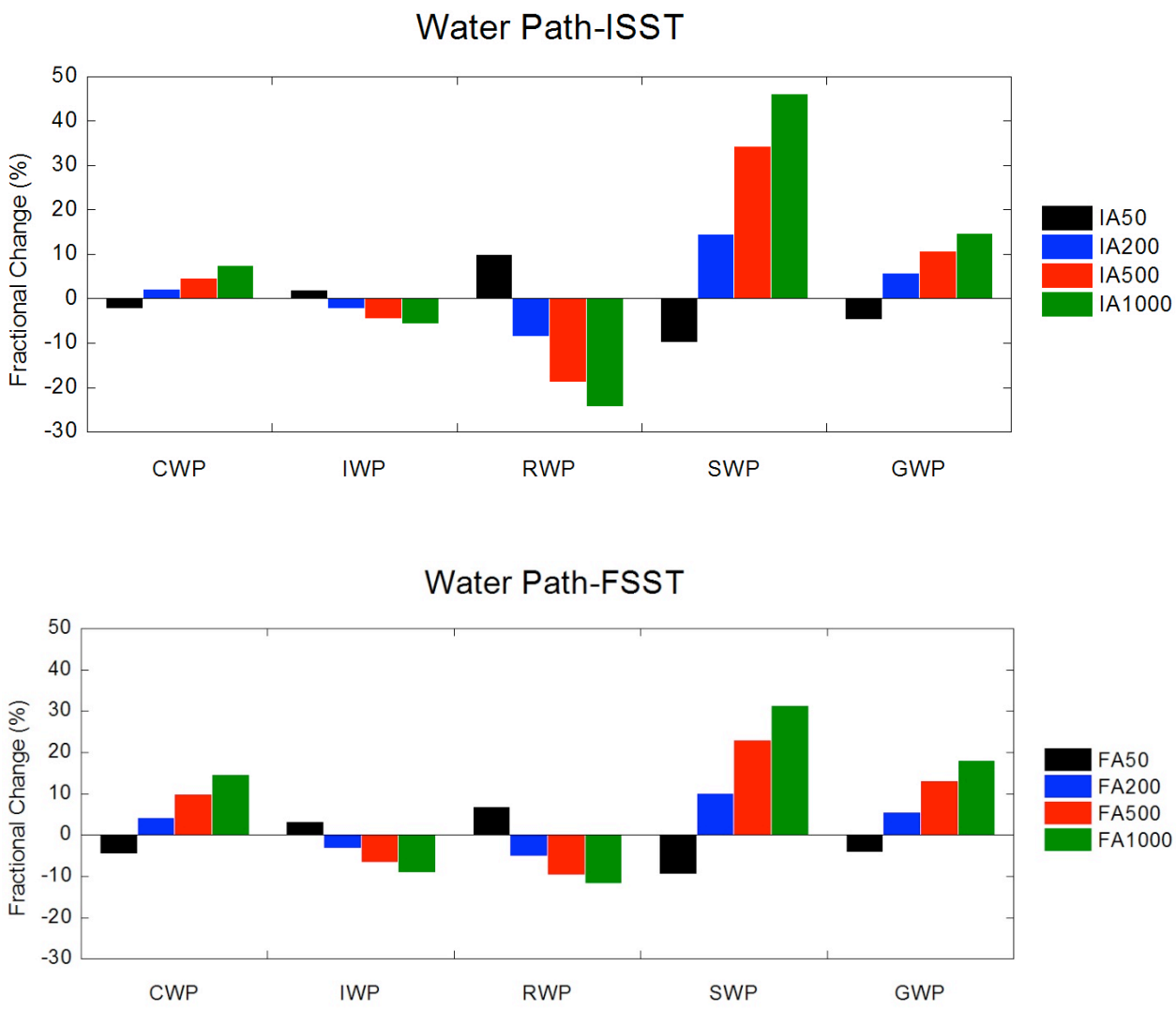

Figure 4.3. Fractional changes of departures (%) of cloud water path. Upper panel: departures of ISSTs from IA100; lower panel: departures of FSSTs from FA100.

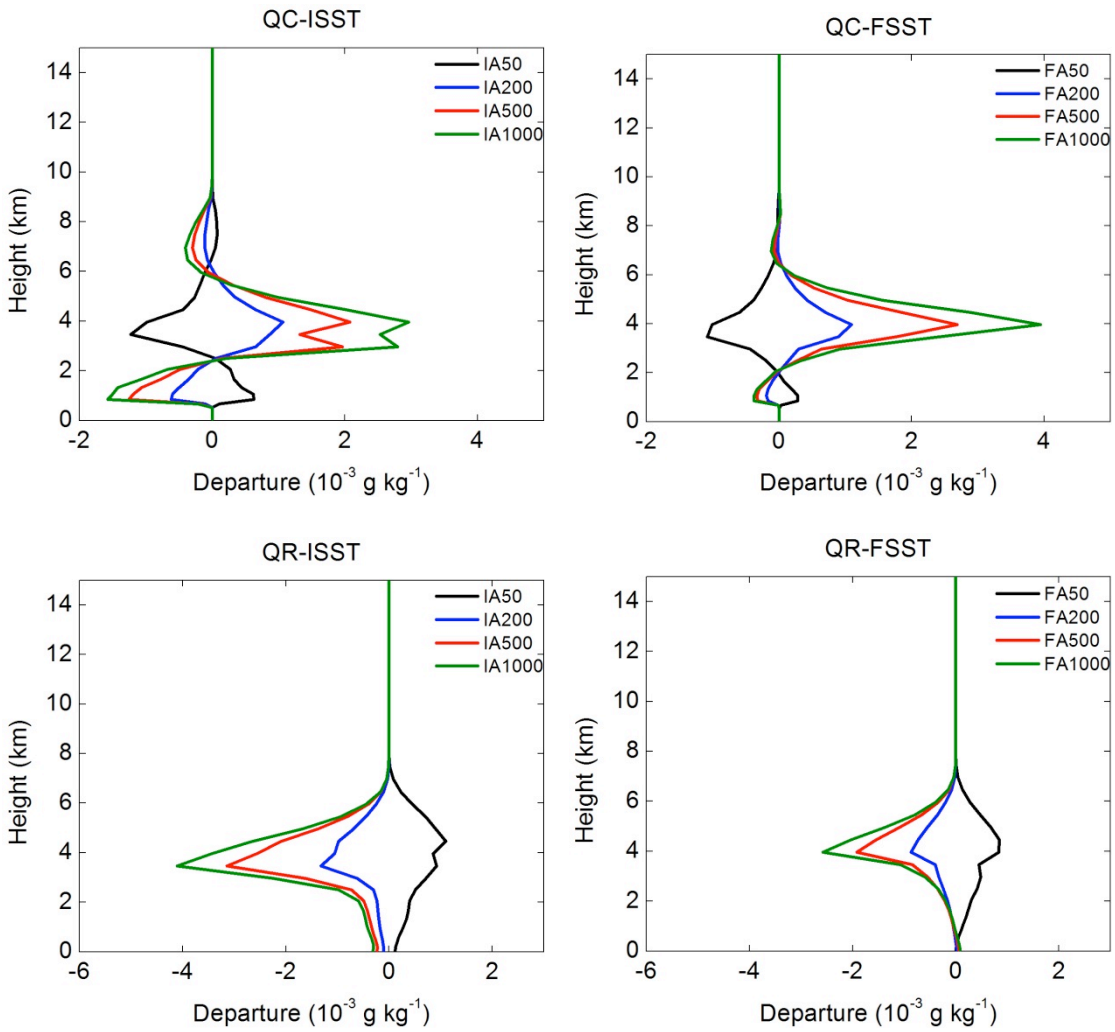

Figure 4.4. Departures of the mixing ratio of cloud liquid water and rainwater. QC: cloud liquid water (10^{-3} g kg^{-1}); QR: rainwater (10^{-3} g kg^{-1}). Left column: interactive SST framework; right column: fixed SST framework.

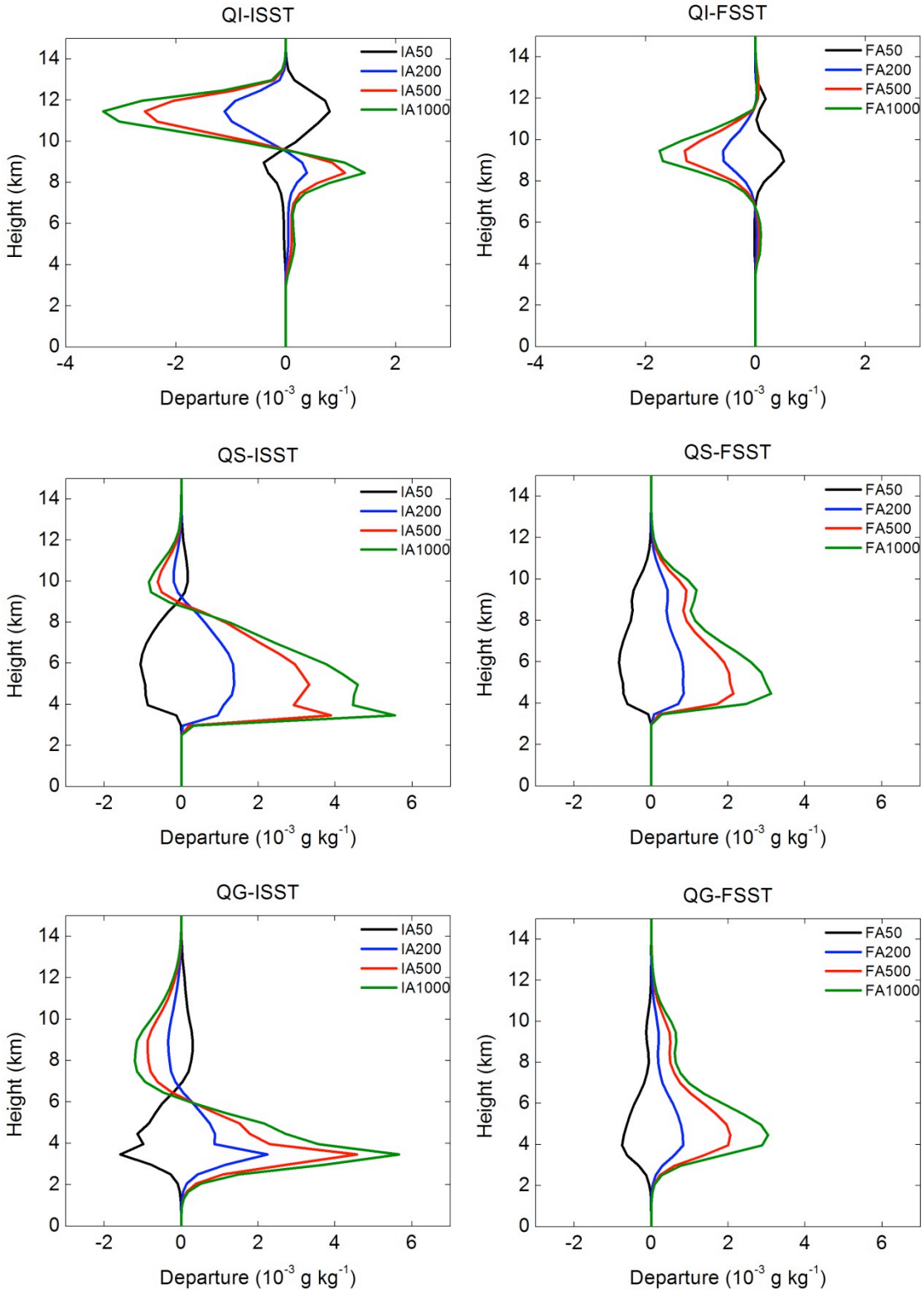

Figure 4.5. Departures of the mixing ratio of cold cloud water. QI: cloud ice (10^{-3} g kg^{-1}); QS: snow (10^{-3} g kg^{-1}); QG: graupel (10^{-3} g kg^{-1}). Left column: interactive SST framework; right column: fixed SST framework.

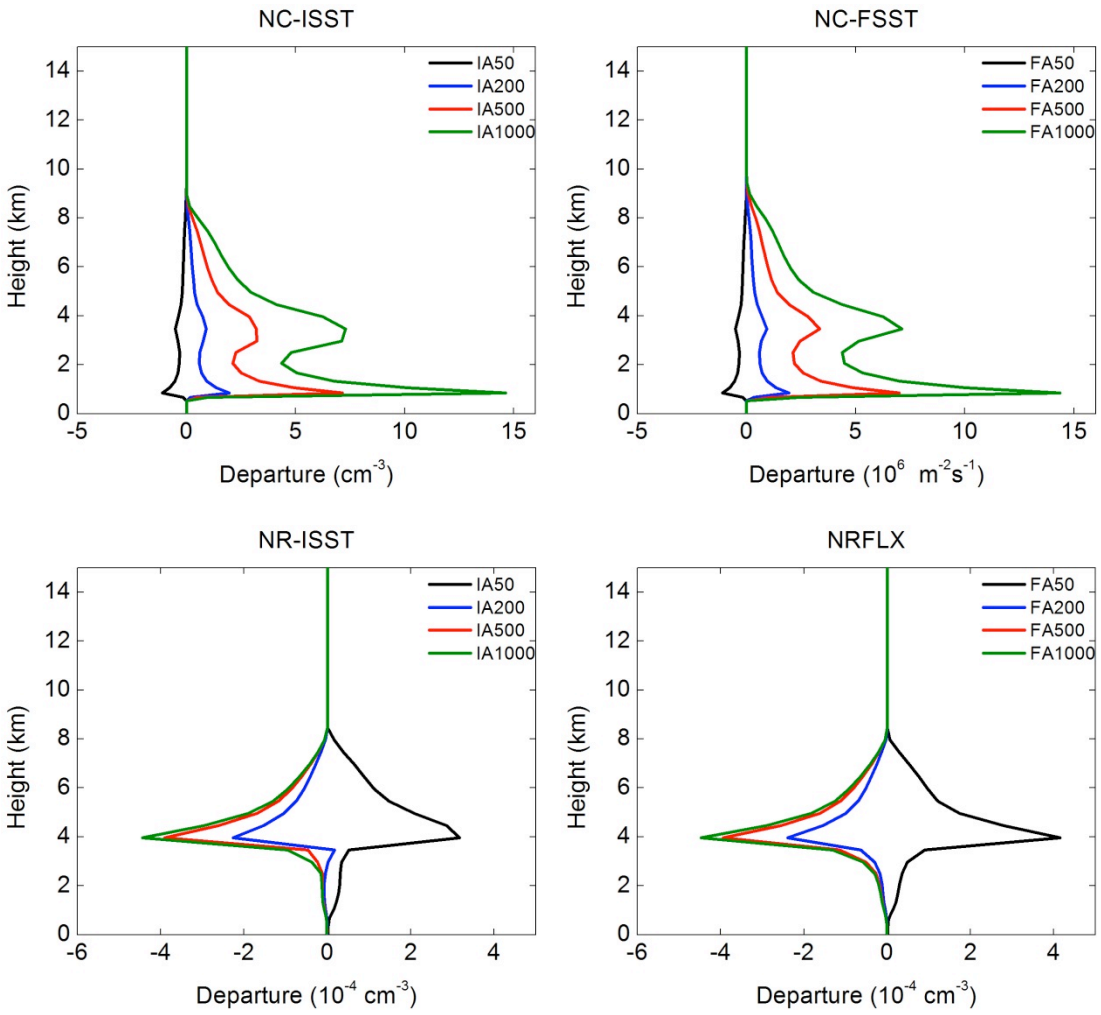

Figure 4.6. Departures of the number concentration of cloud liquid water and rainwater. NC: cloud liquid water (cm^{-3}); NR: rainwater (cm^{-3}) Left column: interactive SST framework; right column: fixed SST framework.

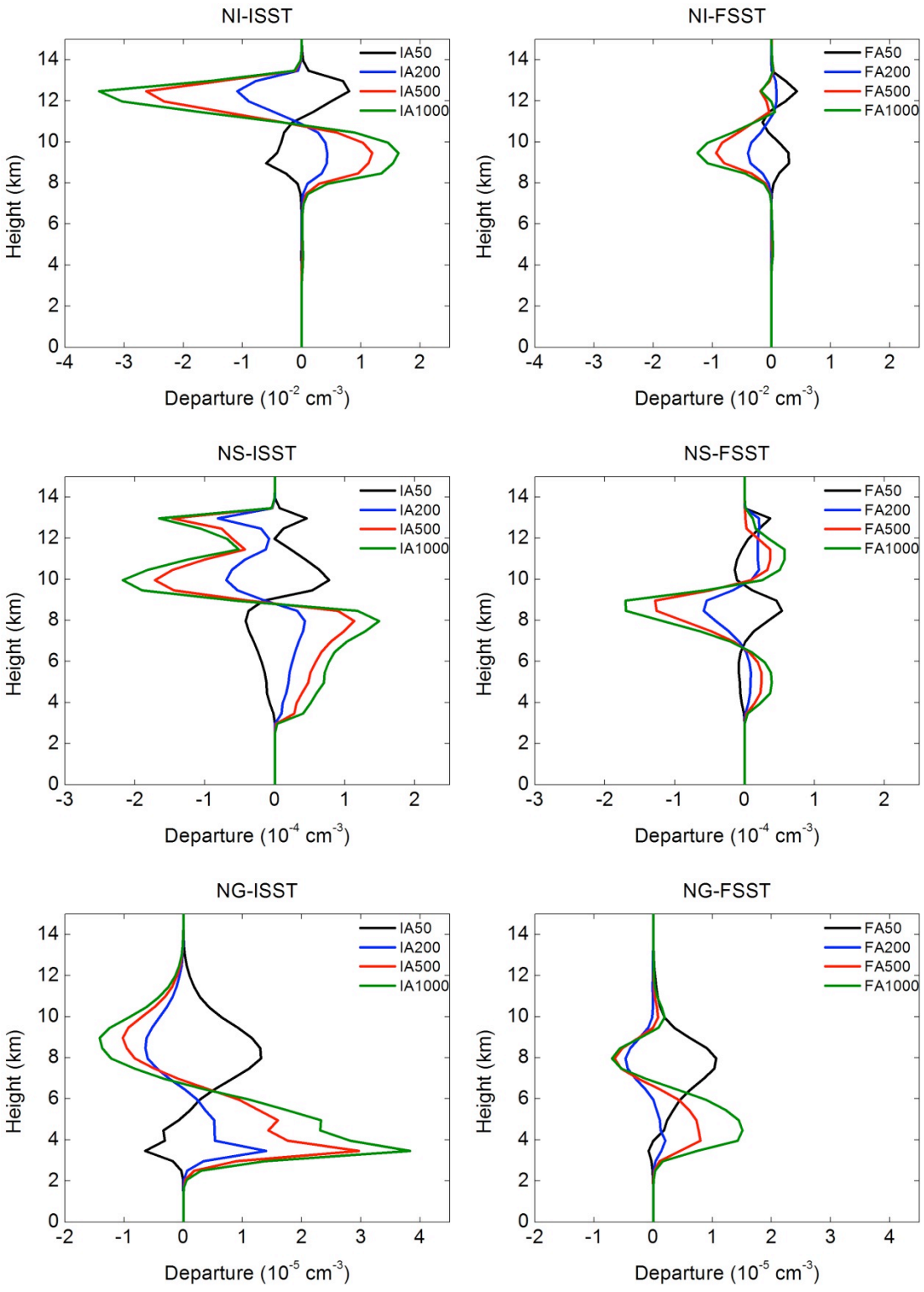

Figure 4.7. Departures of the number concentration of cold cloud water. NI: cloud ice (cm^{-3}); NS: snow (cm^{-3}); NG: graupel (cm^{-3}). Left column: interactive SST framework; right column: fixed SST framework.

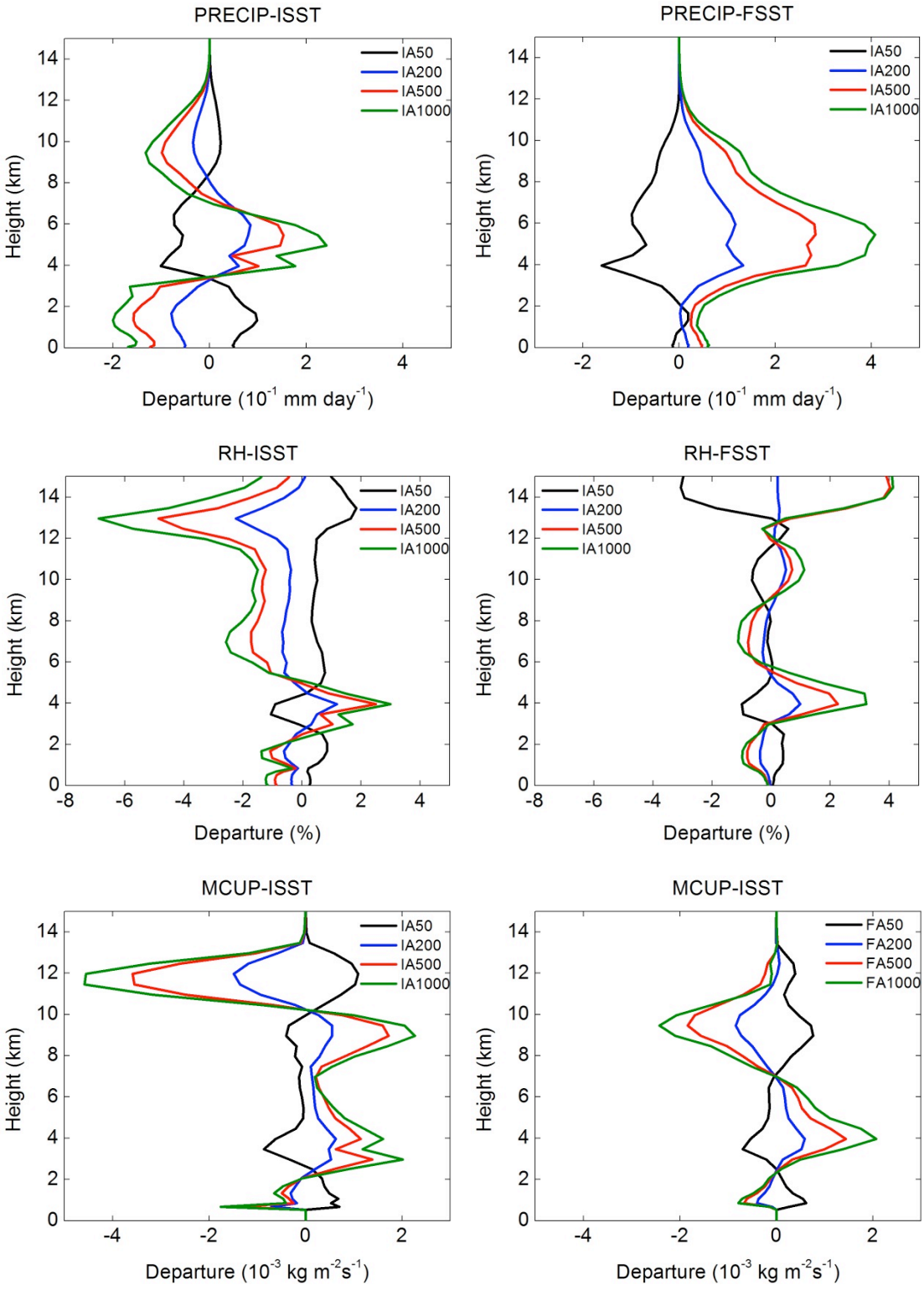

Figure 4.8. Departures of precipitation (top, unit: 10^{-1} mm day^{-1}), relative humidity (middle, unit: %), and updraft cloud mass fluxes (bottom, unit: 10^{-3} kg m^{-2} s^{-1}). Left column: interactive SST framework; right column: fixed SST framework.

CHAPTER 5 CONCLUSION

The impact of aerosol indirect effects (AIEs) has been examined by varying the number concentration of cloud condensation nuclei (CCN) in a three-dimensional cloud-resolving model (CRM), the System for Atmospheric Modeling, with a simple slab ocean model coupled underneath. Two sets of experiments with different sea surface temperature (SST) frameworks are performed over tropical oceans in idealized radiative-convective equilibrium in which no large-scale forcing exists and convection is driven by the constant perpetual insolation.

The simulation results show that AIEs induce a negative impact ranging between 0.5-1.5 K in SST perturbation when the model reaches RCE state. It is this negative feedback that makes the experiments with an interactive SST (ISSTs) predicted from the slab ocean model different from those in the experiments with a fixed SST (FSSTs) framework. A prominent feature is the difference in hydrological cycle. Cooler SST in ISSTs results in less water evaporating from the ocean surface to the atmosphere for activating CCN and forming cloud water whereas evaporation at ocean surface remains the same in fixed SST environment. Therefore, enhancing the CCN amount causes reduction in latent heat flux (LHF) and a negative feedback on precipitable water (PW) and surface precipitation (PREC) in ISSTs while in the case of FSSTs the effects include slightly increased LHF, unchanged PW and a positive feedback on PREC.

The AIEs on the variations of cloud fractions have similar trends in both the experimental sets. Mid-level cloud fraction (MCLD) increases while low-level cloud fraction (LCLD) and high-level cloud fraction (HCLD) decrease with the CCN amount. The decreased LCLD is probably due to smaller evaporation so that fewer CCN are able to get activated as cloud water. The decline in HCLD can be explained by using a dynamical perspective. AIEs induce a weaker updraft cloud mass flux (MCUP) with increasing CCN number concentration such that

suspended cold cloud water (cloud ice, snow, graupel) falls down due to its weight. This mechanism partly explains the increase of MCLD. Another cause for the increasing MCLD is the stronger MCUP at the higher layer of the low level that is responsible for bringing cloud water up to middle level. The overall AIEs on cloud fraction is small (<3%), which is similar to the disturbances in relative humidity profile (<3%, except near and above the cloud anvil) in the model.

From the column-integrated water paths, it is suggested that AIEs tend to enhance cloud liquid water, snow, and graupel but reduce cloud ice and rainwater in both experimental sets. The aerosol second indirect effect manifests itself by the increase of cloud liquid water for both sets. In addition, simulation results demonstrate that the perturbations of mixing ratio profiles of hydrometeors are less sensitive to AIEs in FSSTs than in ISSTs. Moreover, the variation of precipitation flux is associated with the strength of MCUP. Stronger MCUP with respect to the CCN amount at mid-level causes enhanced precipitation flux (PRECIP) within this level whereas weaker MCUP results in reduced PRECIP for both sets. Therefore, relative humidity within the boundary layer is reduced for both sets. Nevertheless, the difference of MCUP below cloud anvil (7-10 km) between ISSTs and FSSTs induces opposite trends of cloud ice in vertical distributions between ISSTs and FSSTs. Enhanced MCUP in ISSTs results in more cloud ice with increasing CCN number concentration while reduced MCUP in FSSTs leads to smaller amount of cloud ice.

In terms of number concentration, both sets show changes in the size distribution of cloud water. In ISSTs, cloud liquid water mixing ratio at lower level decreases with respect to the CCN amount while its number concentration increases. Hence, smaller size of cloud liquid water droplets is expected. Similar responses are found in FSSTs for cloud liquid water at low-level

and snow and graupel at high-level. The overall responses of hydrometeors to AIEs in FSSTs are smaller than those in ISSTs.

The responses of cloud radiative forcing to AIEs show similar patterns in both experimental sets. The shortwave cloud radiative forcing enhances with the CCN amount as more shortwave radiation is scattered. However, reduced longwave cloud radiative forcing (LWCF) is of different mechanism in ISSTs and FSSTs. It is suggested that the cloud amount is responsible for decreasing LWCF in FSSTs whereas SST is the dominant factor in ISSTs. Moreover, the greenhouse warming effect is simulated to be counteracted by AIEs. The cooling effects by AIEs at high CCN burdens can mitigate most of the greenhouse warming effect by doubling carbon dioxide concentration in this work.

According to the simulation results shown previously, this study concludes that using different SST frameworks in a CRM with an idealized RCE framework can influence different feedbacks in climate variations by AIEs, as demonstrated, for example, by different sign of the precipitation feedback.

Bibliography

Abdul-Razzak, H. and S. J. Ghan, 2002: A parameterization of aerosol activation: 3. Sectional representation. *J. Geophys. Res.*, **107**(D3), 4026, doi:10.1029/2001JD000483.

Albrecht, B., 1989: Aerosols, cloud microphysics, and fractional cloudiness. *Science*, **245**, 1227-1230.

Ahrens, C. D. 1998: Essentials of Meteorology, An Invitation to the Atmosphere. Second Edition. Wadsworth Publishing Company, 443pp.

Charlock, T. P. and V. Ramanathan, 1985: The albedo field and cloud radiative forcing produced by a general circulation model with internally generated cloud optics. *J. Atmos. Sci.*, **42**, 1408-1429.

Del Genio, A. D. and A. B. Wolf, 2000: The Temperature Dependence of the Liquid Water Path of Low Clouds in the Southern Great Plains. *J. Climate*, **13**, 3465-3486.

Ghan, S. J., R. C. Easter, E. G. Chapman, H. Abdul-Razzak, Y. Zhang, L. R. Leung, N. S. Laulainen, R. D. Saylor, and R. A. Zaveri, 2001: A physically based estimate of radiative forcing by anthropogenic sulfate aerosol. *J. Geophys. Res.*, **106**, 5279-5293, doi:10.1029/2000JD900503.

Govindasamy, B., S. Thompson, P. B. Duffy, K. Caldeira, and C. Delire, 2002: Impact of geoengineering schemes on the terrestrial biosphere. *Geophys. Res. Lett.*, **29**(22), 2061, doi:10.1029/2002GL015911.

Grabowski, W. W., 2006: Indirect impact of atmospheric aerosols in idealized simulations of convective–radiative quasi equilibrium. *J. Climate*, **19**, 4664-4682.

Grabowski, W. W., P. Bechtold, A. Cheng, R. Forbes, C. Halliwell, M. Khairoutdinov, S. Lang, T. Nasuno, J. Petch, W.-K. Tao, R. Wong, X. Wu, K.-M. Xu, 2006: Daytime convective development over land: A model intercomparison based on LBA observations. *Quart. J. Roy. Meteor. Soc.*, **132**, 317-344.

Hoose, C., J. E. Kristjánsson, J.-P. Chen, and A. Hazra, 2010: A classical-theory-based parameterization of heterogeneous ice nucleation by mineral dust, soot, and biological particles in a global climate model. *J. Atmos. Sci.*, **67**, 2483-2503, doi:10.1175/2010JAS3425.1.

IPCC, 2007: Climate Change 2007: The Physical Science Basis. Contribution of Working Group I to the Fourth Assessment Report of the Intergovernmental Panel on Climate Change [Solomon, S., D. Qin, M. Manning, Z. Chen, M. Marquis, K.B. Averyt, M.Tignor and H.L. Miller (eds.)]. Cambridge University Press, Cambridge, United Kingdom and New York, NY, USA.

Khairoutdinov, M. F. and D. A. Randall, 2003: Cloud-resolving modeling of the ARM summer 1997 IOP: model formulation, results, uncertainties and sensitivities. *J. Atmos. Sci.*, **60**, 607-625.

Kiehl, J. T. and K. E. Trenberth, 1997: Earth's annual global mean energy budget. *Bull. Amer. Meteor. Soc.*, **78**, 197-208.

Kristjánsson, J. E., 2002: Studies of the aerosol indirect effect from sulfate and black carbon aerosols. *J. Geophys. Res.*, **107**(D15), 4246, doi:10.1029/2001JD000887.

Kutzbach, J. E., W. F. Ruddiman, S. Vavrus, and G. Phillippon, 2010: Climate model simulations of anthropogenic influence on greenhouse-induced climate change (early agriculture to modern): the role of ocean feedbacks. *Climatic Change*, **99**, 351-381, doi:10.1007/s10584-009-9684-1.

Liu, X. and J. E. Penner, 2005: Ice nucleation parameterization for global models. *Meteorol. Z.* **14**(4), 499-514, doi:10.1127/0941-2948/2005/0059.

Lohmann, U. and J. Feichter, 2005: Global indirect aerosol effects: a review. *Atmos. Chem. Phys.*, **5**, 715-737, doi:10.5194/acp-5-715-2005.

Lu, M.-L. and J. H. Seinfeld, 2005: Study of the aerosol indirect effect by large-eddy simulation of marine stratocumulus. *J. Atmos. Sci.*, **62**, 3909-3932, doi:10.1175/JAS3584.1.

Menon, Surabi, Anthony D. Del Genio, Dorothy Koch, and George Tselioudis, 2002: GCM Simulations of the Aerosol Indirect Effect: Sensitivity to Cloud Parameterization and Aerosol Burden. *J. Atmos. Sci.*, **59**, 692-713. doi:10.1175/1520-0469(2002)059<0692:GSOTAI>2.0.CO;2

Mitchell, J. F. B. and T. C. Johns, 1997: On modification of global warming by sulfate aerosols. *J. Climate*, **10**, 245-267.

Morrison, H., J. A. Curry, and V. I. Khvorostyanov, 2005: A new double-moment microphysics parameterization for application in cloud and climate models. Part I: Description. *J. Atmos. Sci.*, **62**, 1665-1677.

—— and W. W. Grabowski, 2011: Cloud-system resolving model simulations of aerosol indirect effects on tropical deep convection and its thermodynamic environment. *Atmos. Chem. Phys. Discuss.*, **11**, 10503-10523, doi:10.5194/acp-11-10503-2011.

Nenes, A. and J. H. Seinfeld, 2003: Parameterization of cloud droplet formation in global climate models. *J. Geophys. Res.*, **108**, 4415, doi:10.1029/2002JD002911.

Pincus, R. and M. B. Baker, 1994: Effect of precipitation on the albedo susceptibility of clouds in the marine boundary layer. *Nature*, **372**, 250-252, doi:10.1038/372250a0.

Pruppacher H. R. and J. D. Klett, 1997: Microphysics of clouds and precipitation. Kluwer Academic Publishers, Boston, USA, 954 pp.

Quaas, J., Y. Ming, S. Menon, T. Takemura, M. Wang, J. E. Penner, A. Gettelman, U. Lohmann, N. Bellouin, O. Boucher, A. M. Sayer, G. E. Thomas, A. McComiskey, G. Feingold, C. Hoose, J. E. Kristjánsson, X. Liu, Y. Balkanski, L. J. Donner, P. A. Ginoux, P. Stier, B. Grandey, J. Feichter, I. Sednev, S. E. Bauer, D. Koch, R. G. Grainger, A. Kirkevåg, T. Iversen, Ø. Seland, R. Easter, S. J. Ghan, P. J. Rasch, H. Morrison, J.-F. Lamarque, M. J. Iacono, S. Kinne, and M. Schulz, 2009: Aerosol indirect effects general circulation model intercomparison and evaluation with satellite data. *Atmos. Chem. Phys.*, **9**, 8697-8717, doi:10.5194/acp-9-8697-2009.

Rasch, P. J., J. Latham, and C.-C. Chen, 2009: Geoengineering by cloud seeding: influence on sea ice and climate system. *Environ. Res. Lett.*, **4**:045112, doi:10.1088/1748-9326/4/4/045112.

Rossow, W. B. and R. A. Schiffer, 1999: Advances in understanding clouds from ISCCP. *Bull. Amer. Meteorol. Soc.*, **80**, 2261-2288.

Rotstayn, L. D. and J. E. Penner, 2001: Indirect aerosol forcing, quasi forcing, and climate response. *J. Climate*, **14**, 2960-2975.

—— and Y. Liu, 2009: Cloud droplet spectral dispersion and the indirect aerosol effect: comparison of two treatments in a GCM. *Geophys. Res. Lett.*, **36**, L10801, doi:10.1029/2009GL038216.

—— and U. Lohmann, 2002: Tropical rainfall trends and the indirect aerosol effect. *J. Climate*, **15**, 2103-2116.

Satoh, M., Shin-ichi Iga, Hirofumi Tomita, Yoko Tsushima, and Akira, T. Noda, 2011: Response of upper clouds in global warming experiments obtained using a global nonhydrostatic model with explicit cloud processes. *J. Climate*. [Early online release]. doi: 10.1175/JCLI-D-11-00152.1.

Stephens, G. L., A. Slingo, M. J. Webb, P. J. Minnett, P. H. Daum, L. Kleinman, I. Wittmeyer, and D. A. Randall, 1994: Observations of the Earth's Radiation Budget in relation to atmospheric hydrology. 4. Atmospheric column radiative cooling over the world's oceans. *J. Geophys. Res.*, **99**, 18585-18604.

——, N. B. Wood, and L. A. Pakula, 2004b: On the radiative effects of dust on tropical convection. *Geophys. Res. Lett.*, **31**, L23112, doi:10.1029/2004GL021342.

——, S. van den Heever, and L. Pakula, 2008: Radiative–convective feedbacks in idealized states of radiative–convective equilibrium. *J. Atmos. Sci.*, **65**, 3899-3916.

Tao, W-K., J. Simpson, C-H. Sui, C-L. Shie, B. Zhou, K. M. Lau, and M. Moncrieff, 1999: Equilibrium States Simulated by Cloud-Resolving Models. *J. Atmos. Sci.*, **56**, 3128-3139.

——, S. Lang, J. Simpson, C.-H. Sui, B. Ferrier, and M.-D. Chou, 1996: Mechanisms of cloud–radiation interaction in the Tropics and midlatitudes. *J. Atmos. Sci.*, **53**, 2624-2651.

——, X. Li, A. Khain, T. Matsui, S. Lang, and J. Simpson, 2007: Role of atmospheric aerosol concentration on deep convective precipitation: cloud-resolving model simulations. *J. Geophys. Res.*, **112**, D24S18, doi:10.1029/2007JD008728.

Taylor, K. E. and J. E. Penner, 1994: Response of the climate system to atmospheric aerosols and greenhouse gases. *Nature*, **369**, 734-737, doi:10.1038/369734a0.

Tompkins, A. M., 2000: The impact of dimensionality on long-term cloud resolving model simulations. *Mon. Wea. Rev.*, **128**, 1521-1535.

—— and G. C. Craig, 1998a: Radiative-convective equilibrium in a three-dimensional cloud ensemble model. *Quart. J. Roy. Meteor. Soc.*, **124**, 2073-2097.

—— and ——, 1999: Sensitivity of Tropical convection to sea surface temperature in the absence of large-scale flow. *J. Climate*, **12**, 462-476.

Twomey, S., 1959: The nuclei of natural cloud formation. Part II: the supersaturation in natural clouds and the variation of cloud droplet concentrations. *Pure and Applied Geophysics*, **43**, 243-249.

——, 1974: Pollution and the planetary albedo. *Atmos. Environ.*, **8** (12), 1251-1256.

van den Heever, S. C., G. L. Stephens, and N. B. Wood, 2011: Aerosol indirect effects on tropical convection characteristics under conditions of radiative-convective equilibrium. *J. Atmos. Sci.*, **68**, 699-718. doi:10.1175/2010JAS3603.1.

Wang, C., 2005: A modeling study of the response of tropical deep convection to the increase of cloud condensation nuclei concentration: 1. Dynamics and microphysics. *J. Geophys. Res.*, **110**, D21211. doi:10.1029/2004JD005720.

Xu, K.-M., R. T. Cederwall, L. J. Donner, W. W. Grabowski, F. Guichard, D. E. Johnson, M. Khairoutdinov, S. K. Krueger, J. C. Petch, D. A. Randall, C. J. Seman, W.-K Tao, D. Wang, S. C. Xie, J. J. Yio, and M.-H. Zhang, 2002: An intercomparison of cloud-resolving models with the Atmospheric Radiation Measurement summer 1997 intensive observation period data. *Quart. J. Roy. Meteor. Soc.*, **128**, 593-624.

—— and D. A. Randall, 1999: A sensitivity study of radiative–convective equilibrium in the tropics with a convection-resolving model. *J. Atmos. Sci.*, **56**, 3385-3399.

Appendix

Table A. The simulation results for all experiments.

Case	SST (K)	PW (mm)	PREC (mm day^{-1})	SHF (W m^{-2})	LHF (W m^{-2})
IA50	300.52	40.82	3.17	10.25	92.30
IA100	300.09	39.20	3.12	10.33	90.82
IA200	299.60	37.50	3.07	10.45	89.27
IA500	298.95	35.43	3.00	10.56	87.17
IA1000	298.55	34.27	2.95	10.61	85.81
I2CO2	302.01	47.05	3.37	9.77	97.94
FA50	300.00	38.92	3.10	10.32	89.96
FA100	300.00	38.91	3.11	10.33	90.36
FA200	300.00	38.91	3.13	10.40	90.91
FA500	300.00	38.90	3.16	10.52	91.72
FA1000	300.00	38.98	3.17	10.57	92.08

Case	LWNT (W m^{-2})	LWNTC (W m^{-2})	SWNT (W m^{-2})	SWNTC (W m^{-2})	LWCF (W m^{-2})	SWCF (W m^{-2})
IA50	222.08	264.28	222.57	240.91	42.20	222.08
IA100	221.87	263.73	222.21	240.89	41.86	221.87
IA200	221.74	263.03	221.92	240.88	41.29	221.74
IA500	221.29	262.10	221.27	240.85	40.81	221.29
IA1000	220.77	261.52	220.68	240.84	40.75	220.77
I2CO2	222.18	261.23	222.87	240.96	39.05	222.18
FA50	221.16	263.68	222.50	240.89	42.52	221.16
FA100	221.68	263.55	222.20	240.89	41.86	221.68
FA200	222.41	263.51	221.94	240.89	41.10	222.41
FA500	223.57	263.41	221.59	240.89	39.84	223.57
FA1000	223.94	263.32	221.21	240.89	39.38	223.94

Table A (continued). The simulation results for all experiments.

Case	CWP ($g\ m^{-2}$)	IWP ($g\ m^{-2}$)	RWP ($g\ m^{-2}$)	SWP ($g\ m^{-2}$)	GWP ($g\ m^{-2}$)
IA50	31.44	17.13	34.62	24.13	42.34
IA100	32.13	16.88	31.47	26.82	44.59
IA200	32.86	16.42	28.79	30.61	46.94
IA500	33.62	16.02	25.54	35.91	49.25
IA1000	34.52	15.82	23.84	39.00	50.90
I2CO2	33.66	16.38	34.86	24.39	45.81
FA50	30.57	17.41	33.45	24.29	42.62
FA100	32.04	16.93	31.31	26.90	44.56
FA200	33.42	16.35	29.70	29.53	46.90
FA500	35.21	15.74	28.28	32.97	50.24
FA1000	36.71	15.32	27.59	35.24	52.42

Case	LCLD (%)	MCLD (%)	HCLD (%)	TCLD (%)
IA50	3.04	2.61	51.86	57.51
IA100	2.88	2.67	51.81	57.36
IA200	2.81	2.77	51.45	57.02
IA500	2.76	2.89	50.62	56.27
IA1000	2.73	3.14	51.36	57.22
I2CO2	3.20	2.53	49.92	55.64
FA50	2.93	2.55	51.71	57.20
FA100	2.87	2.66	51.81	57.34
FA200	2.85	2.79	51.44	57.08
FA500	2.85	2.88	50.21	55.94
FA1000	2.82	3.02	50.19	56.04